Nuclear medicine imaging for bone metastases assessment: what else besides bone scintigraphy in the era of personalized medicine?

Eric Ouvrard[1]*, Ashjan Kaseb[1,2], Nathan Poterszman[1],
Clémence Porot[3], Francois Somme[1] and Alessio Imperiale[1,4]

[1]Nuclear Medicine and Molecular Imaging, Institut de Cancérologie Strasbourg Europe (ICANS),
University Hospitals of Strasbourg, University of Strasbourg, Strasbourg, France, [2]Radiology, College
of Medicine, University of Jeddah, Jeddah, Saudi Arabia, [3]Radiopharmacy, Institut de Cancérologie
Strasbourg Europe (ICANS), Strasbourg, France, [4]IPHC, UMR 7178, CNRS/Unistra, Strasbourg, France

Accurate detection and reliable assessment of therapeutic responses in bone metastases are imperative for guiding treatment decisions, preserving quality of life, and ultimately enhancing overall survival. Nuclear imaging has historically played a pivotal role in this realm, offering a diverse range of radiotracers and imaging modalities. While the conventional bone scan using ^{99m}Tc marked bisphosphonates has remained widely utilized, its diagnostic performance is hindered by certain limitations. Positron emission tomography, particularly when coupled with computed tomography, provides improved spatial resolution and diagnostic performance with various pathology-specific radiotracers. This review aims to evaluate the performance of different nuclear imaging modalities in clinical practice for detecting and monitoring the therapeutic responses in bone metastases of diverse origins, addressing their limitations and implications for image interpretation.

KEYWORDS

bone metastases, bone scan, ^{99m}Tc, 18 F-FDG, 18 F-fluorocholine, 68Ga-DOTA, 18F-DOPA, 18F-NaF?

Introduction

The skeleton is the most common organ affected by metastatic spread in solid tumors, notably in breast and prostate carcinomas. Given the prevalence of bone metastasis in specific cancers, vigilant monitoring for bone involvement and prompt intervention are integral aspects of cancer care for individuals at risk. When cancer cells invade the bones, they can disrupt normal bone function, leading to symptoms like bone pain, pathological fractures, and complications related to modifications in bone marrow function. Complications associated with bone metastases are collectively referred to as skeletal-related events (SRE), primarily encompassing pathological fractures, spinal cord compression, and hypercalcemia. SREs are remarkably common among metastatic patients, occurring on average every 3–6 months (1). Early diagnosis and assessment of therapeutic responses to bone metastases are crucial for guiding cancer treatment strategies and minimizing the occurrence of SREs. Managing bone metastasis often involves a range of treatments, including surgery, radiation therapy,

bisphosphonate medications, targeted therapies, and palliative care, aimed at alleviating symptoms and enhancing the patient's quality of life.

In the last decade, significant progress has been made in understanding the tumoral burden on the skeleton. The intricate dependence and interaction between cancer cells and the bone microenvironment has been emphasized. Normal bone tissue undergoes constant dynamic remodeling, where the functions of osteoclastic resorption and osteoblastic production are intricately balanced. Disruption of this delicate equilibrium by cancer cells results in the production of various patterns of bone lesions (2). Skeletal metastases are commonly classified as osteolytic, sclerotic, or osteoblastic based on the radiographic appearance of the lesion. However, schematic dichotomous differentiation is not always possible, as lesions may exhibit both morphological types (mixed metastasis). Predominance of bone resorption mechanisms, generally mediated by activated osteoclasts, leads to the detection of destructive bone lesions, giving metastasis a lytic aspect. Lytic metastases are most common and prevalent in breast, lung, thyroid, renal, and gastro-intestinal malignancies. Myeloma almost always causes osteolytic metastases. Conversely, amplified osteoblastic activity, associated with abnormal formation of frequently unstructured new bone, is prevalent in metastases with a sclerotic appearance. While prostate carcinoma is the main cause of osteoblastic metastases, breast, lung, and neuroendocrine tumors can also cause sclerotic bone lesions.

Metastatic spread predominantly targets skeletal segments rich in highly vascularized red marrow deposits. The physical properties of circulation in these areas, characterized by vascular sinusoids with endothelial cells lacking a basement membrane, facilitate tumor extravasation (3). Consequently, the axial skeleton, ribs, long bones, and vertebral column are commonly affected sites of metastasis. The metastatic process involves a complex multistep interaction between malignant cells and the host microenvironment. Early stages include local tumoral proliferation, cellular detachment, and invasion of organ stroma. Systemic circulation is reached through the penetration of cells into blood vessels and/or lymphatic structures. Adhesion and extravasation into the target organ (bone microenvironment) are crucial stages in metastatic development. Cell adhesion molecules (CAM), expressed on the surface of tumoral cells and in the metastatic site, play a key role in this process, supporting the nonrandom hypothesis of tumor metastases (4, 5). Integrins, a common CAM family, facilitate tumoral cell adhesion to vascular endothelial structures. The rupture of blood vessel basement membranes, induced by the secretion of proteolytic enzymes (i.e., type IV collagenase) by tumoral and host cells, predicts tumoral extravasation through chemotaxis. Subsequent interaction with the microenvironment, involving osteolytic and osteoblastic phenomena, occurs (6). The development of bone metastases can be summarized in four steps (7): (a) bone colonization by circulating tumor cells, formation of a premetastatic niche in the bone marrow, extravasation of circulating tumor cells influenced by pro-migratory and pro-inflammatory tumor-secreted molecules, and tumor cell engraftment; (b) cancer cell dormancy, as the bone marrow environment limits cancer cell proliferation; (c) reactivation of dormant cells after acquiring appropriate genetic mutations allowing them to express bone-specific proteins; (d) disruption of bone homeostasis through the secretion of factors that stimulate or inhibit osteoclast and osteoblast activity, leading to the development of metastases.

Nuclear medicine imaging

Nuclear medicine imaging has been a cornerstone in the diagnosis and management of bone metastases, playing a vital role in the field of oncology (8, 9). This medical imaging modality provides a diverse array of radiotracers meticulously crafted to address various clinical scenarios. Furthermore, nuclear imaging continues to evolve with technological advancements, making it an essential tool in the detection and monitoring of bone metastases, a common manifestation of advanced cancer. Nuclear medicine enables a non-invasive characterization of tumoral functional status and variability at the molecular and cellular level, examining the uptake intensity and kinetics of several radiotracers. Molecular imaging techniques are highly sensitive, allowing the detection of diseases at the initial stages. To enhance diagnostic accuracy, the integration of anatomical and functional imaging is often achieved through "hybrid" modalities such as Positron Emission Tomography/Computed Tomography (PET/CT) and Single Photon Emission Computed Tomography/Computed Tomography (SPECT/CT) devices (10). While PET/MRI hybrid systems are now available, their role is still being established, and their clinical routine availability is limited.

Understanding the pathophysiology of bone metastases is crucial for comprehending the deployment of various nuclear imaging modalities and their respective strengths and limitations. Nuclear imaging for bone metastasis detection relies on different radiotracers that offer insights into tumor activity, either directly (e.g.,^{18}F-fluorodeoxyglucose (^{18}F-FDG), ^{18}F-Fluorocholine (^{18}F-FCH), $^{18F-or}$ ^{68}Ga-radiolabeled prostate-specific membrane antigen (PSMA), ^{18}F-Fluoro-dihydroxyphenylalanine (^{18}F-DOPA), radiolabeled somatostatin analogs like ^{68}Ga-DOTA-peptides) or indirectly, often through the assessment of osteoblastic markers [bisphosphonates labeled with ^{99m}Tc, and ^{18}F-Fluoride (^{18}F-NaF)].

In this narrative review, we will explore the historical significance and the ever-evolving landscape of nuclear imaging in the diagnosis and management of bone metastases, highlighting its pivotal role in improving patient care and outcomes.

Bone scan: the historical cornerstone in the management of bone metastases

The predominant nuclear imaging technique utilized in the management of bone metastases is bone scintigraphy, commonly referred to as a bone scan (BS). Typically, this involves planar scintigraphy followed by tomographic acquisition, often combined with CT. A ^{99m}Tc-labeled bisphosphonate is intravenously administered for this procedure. This radiotracer binds to the mineralization front of hydroxyapatite crystals and the osteocyte gap boundary (11). Consequently, the uptake of the radiotracer is directly influenced by both osteoblastic activity and regional blood flow guiding it to its target.

The BS serves as a valuable tool for estimating the metabolic activity of the skeleton and identifying lesions that cause distinct alterations in physiological bone turnover, even in pre-radiological phases. In contrast, plain radiographs require a 30–50% bone mineral loss before visualizing bone metastases (12). The BS offers the

advantage of conducting a whole-body exploration in a short time, with low patient irradiation and high sensitivity for osteoblastic phenomena (13). However, its major drawbacks include a lack of specificity and a low sensitivity for bone lesions with a prevalent osteolytic pattern. Despite the emergence of PET/CT and MRI, the BS still has important indications in oncology, particularly in the work-up of metastatic breast cancer as per the 2021 European Society of Medical Oncology (ESMO) guidelines (14), advanced prostate cancer according to the 2020 American Society of Clinical Oncology guidelines (15), or moderate to high-risk prostate cancer according to the 2020 ESMO guidelines (16). In the following section on the BS, we will focus on these two types of tumors, discussing their performance, limitations, and potential complementarity with other available diagnostic methods.

Diagnosis of bone lesions

Several studies have conducted a comparative analysis of the diagnostic accuracy between BS and ^{18}F-FDG PET/CT in breast cancer. A 2008 meta-analysis revealed a pooled sensitivity for BS of 88% and a specificity of 87% (17). A 2012 systematic review, focusing on newly diagnosed breast cancers, reported a median sensitivity of 98% and a specificity of 93.5% (18). However, within these high median rates, there is variability among studies, with some reporting lower sensitivities. In a more recent 2017 study using histology, clinical, and imaging follow-up as a reference, a sensitivity of 89% was found for BS. Notably, different sensitivities were observed based on the phenotype of metastases, with a sensitivity of 94–100% for osteoblastic and mixed metastases, 90% for osteolytic, and 70% for infraradiologic metastases. In a recent study comparing ^{18}F-FDG and BS, a sensitivity of about 51% was found for BS in detecting osteolytic lesions (19). These lower sensitivities are also observed in renal carcinoma, which is mainly responsible for lytic metastases (20–22). Concerning lung cancer, three meta-analyses comparing bone scans to ^{18}F-FDG PET with or without CT reported sensitivities and specificities ranging from 86 to 91.8% and 68.8 to 88%, respectively (23–25). All these three meta-analyses concluded to the superiority of ^{18}F-FDG imaging.

In the context of prostate cancer, a recent meta-analysis conducted in 2023, comprising 31 studies, compared radiolabeled PSMA PET/CT with conventional imaging for the initial staging of intermediate-to-high-risk patients. The meta-analysis reported a pooled sensitivity of 73% and a specificity of 79.1% (26). The sensitivity of BS is impacted by the low detection rate of lytic lesions, which are more common in high-risk patients, and by metastases smaller than the spatial resolution of the gamma camera (even with SPECT acquisitions), both often detected by PSMA PET/CT (26). These variations in sensitivity based on metastasis phenotype should be considered when encountering lytic lesions without significant uptake. Additionally, the effectiveness of BS is limited by their inability to provide specific information about bone lesions, posing challenges in differentiating between benign bone tumors and metastases based solely on uptake patterns. To interpret results accurately and consider the possibility of a bone biopsy, a comprehensive understanding of the distinctive morphological traits of various benign bone tumors and their corresponding uptake levels in a BS is essential (10).

Follow-up during treatment

Assessing the therapeutic response using bone scintigraphy can be intricate and requires an understanding of various phenomena associated with the evolution of bone metastases in response to treatment (8, 27, 28). Factors such as flare-ups, changes in the density of bone metastases, and potential interferences from bisphosphonates and anti-RANKL agents can complicate the interpretation of results during systemic treatment for patients with bone metastases. These complexities may lead to misleading conclusions about tumor progression or response to the treatment.

Flare-up phenomenon

Flare-up is characterized by an apparent progression of bone metastases, such as an increase in the number of bone lesions or enlargement and heightened uptake intensity of known lesions, following the initiation of systemic therapy. This phenomenon is not indicative of actual disease progression. The main mechanisms proposed to explain flare-ups include bone formation replacing necrotic tumoral tissue and inflammatory responses secondary to the destruction of tumor cells. Additionally, in patients with prostate cancer treated with abiraterone, a direct anti-osteolytic and pro-osteoblastic effect of the drug has been observed, leading to increased uptake of bone-targeting radiotracers (29). Flare-up is typically observed in BS imaging but has also been reported in patients undergoing PET/CT with several radiotracers (30–33). This phenomenon is commonly seen within the first 6 months following the introduction of hormonal drugs and chemotherapy in prostate and breast cancer patients (27). It has also been documented in non-small cell lung cancer patients treated with gefitinib between 29 and 77 days after the initiation of treatment (34). To minimize misinterpretation, it is recommended to wait for a period of 6 months after the initiation of systemic treatment before assessing the therapeutic response. In patients with metastatic prostate cancer, the Prostate Cancer Working Group 3 (PCWG3) has established criteria to differentiate between flare-up and real disease progression (35). According to these criteria, a 2 + 2 rule is applied: over the first 24 weeks, patients should undergo a BS every 8–9 weeks. Genuine progression is defined by the identification of at least two new lesions on an initial BS, accompanied by the detection of at least two additional lesions on a subsequent BS.

In the era of SPECT/CT technology, there was optimism that the CT component would provide valuable insights for the interpretation of BS. Unfortunately, it turns out that CT is also susceptible to flare-ups. Among patients with castrate-resistant prostate cancer receiving treatment, a noteworthy 21% experienced an exacerbation of metastatic bone conditions when assessed through a 3 months CT scan, despite observing improvements in their PSA levels. Approximately one-third of these patients did not exhibit any CT progression when re-evaluated 6 months after the start of treatment (36). In addition, the flare-up phenomenon can also be observed during morphological and diffusion MRI sequences, potentially leading to diagnostic errors if not recognized. Finally, despite the challenges in assessing the therapeutic response induced by the flare-up phenomenon, some authors suggest considering it to increase the sensitivity and specificity of bone scintigraphy after treatment

initiation, with potential therapeutic impact, particularly on tumors initially staged as localized (37).

Decreasing density of bone metastases

Similar to how an increase in the density of sclerotic bone metastases can be associated with either a therapeutic response or progression, studies in prostate cancer under androgen deprivation therapy have found that a decrease in the density of initially sclerotic bone metastases and a reduction in the uptake of bone-targeting agents can also be indicative of both scenarios (Figure 1) (38, 39). This may be attributed to the suppression of the osteoblastic effect of testosterone in the event of a therapeutic response or the progression towards predominant lytic phenomena following the acquisition of resistance to hormonal therapy (38). In prostate cancer, this limitation could be overcome by the advent of radiolabeled PSMA PET/CT. In a retrospective analysis involving prostate cancer patients receiving androgen deprivation therapy, findings revealed that among the 65 patients with bone metastases who underwent ^{68}Ga-PSMA PET/CT scans, 15 individuals (23%) displayed a decrease in the density of their bone metastases. Among the 37 lesions that exhibited reduced density, 21 (57%) were negative on PET scans, while 16 (43%) had intense ^{68}Ga-PSMA uptake (38). Significantly, PET scans did not detect any positive findings in the bone lesions of patients who exhibited a treatment response.

Interference of bisphosphonate and anti-RANKL treatment

The resemblance between bisphosphonates utilized in BS (such as ^{99m}Tc-HDP, ^{99m}Tc-HMDP, ^{99m}Tc-MDP) and those employed for therapeutic applications could give rise to competition for binding sites and reduced tumoral uptake of the radiotracer. This hypothesis was supported by several clinical observations noting a reduced skeletal uptake as soon as 24 h after administration of etidronate (40–43). The persistence of this effect could be observed for a duration of 15 days, as evidenced by consecutive serial BS (42). However, besides small effective sizes, inconsistencies in scanning timing, and the absence of systematic control scintigraphy before bisphosphonate administration, all the reported clinical cases involved etidronate, which is not the main bisphosphonate used in clinical routine.

Three prospective studies addressed this question by comparing bone scintigraphy before and after the administration of different bisphosphonates such as pamidronate, clodronate, zoledronic acid, and alendronate, revealing no notable reduction in bone uptake observed during the course of treatment (44–46). In one autopsy series, the concordance between bone scintigraphy results and bone histology was investigated in 11 patients who had succumbed to androgen-independent prostate cancer. Among them, five had received pamidronate treatment (47). No significant difference in the detection of bone metastases was reported in patients treated with pamidronate.

Today, denosumab, an anti-RANKL that inhibits osteoclast function, has largely replaced bisphosphonate in patients with bone metastases to reduce the risk of SREs. Very few data are available to evaluate its impact on bone scintigraphy. One review reported a case of almost normalization of bone metastases uptake after the introduction of denosumab, despite the rise in biological tumor markers (48). A more recent study compared the uptake intensity of ^{18}F-NaF between patients treated by denosumab and a control group using cervical vertebrae as a reference, showing no significant difference (49).

FIGURE 1
^{99m}Tc-HMDP SPECT/CT in a first patient with a bone metastatic prostate adenocarcinoma under first generation hormonotherapy for 2 years, showing a right posterior iliac sclerotic bone metastasis with a high uptake (A,B). Routine follow-up 6 months later showed shading of the iliac metastasis and less intense uptake (E,F), linked to a progression confirmed by a rising PSA and subsequent imaging. ^{99m}Tc-HMDP SPECT/CT in a second patient with a bone metastatic breast invasive lobular carcinoma, displaying a vertebral sclerotic metastasis with a high uptake at initial staging (C,D). Routine follow-up 12 months later showed a shadowing of the metastasis and a less intense uptake (G,H), indicative of a therapeutic response confirmed by clinical evolution and subsequent imaging.

Response to treatment

The limitations of BS mentioned earlier, along with the gamma camera's lower spatial resolution compared to PET/CT (approximately 15 mm for SPECT/CT vs. 4 mm for last-generation PET/CT devices), its reduced sensitivity in detecting purely lytic lesions, and the time interval between an effective therapeutic response and the decline in bone-targeting radiotracer uptake, collectively diminish the effectiveness of BS in evaluating treatment responses. Additionally, bone scintigraphy is constrained by moderate interobserver agreement (50).

However, due to their accessibility and relatively low cost compared to PET/CT and whole-body MRI, BS are still widely used in the follow-up of metastatic patients. In this context, caution should be exercised when interpreting changes in BS; confirmation around 8 weeks after the first equivocal BS should be carried out, or further investigations with other imaging modalities may be requested. In the specific case of prostate cancer, the previously mentioned PCWG3 criteria can be applied (35). However, this semi-quantitative method does not account for lesions that are increasing in size and can therefore be misleading for some progressive patients. To address this limitation, an alternative quantitative approach known as the BS Index (BSI), specifically designed for prostate cancer, can be employed (51). It represents the fraction of the total skeleton involved in metastases. However, it remains a time-consuming process and is therefore not easily utilized in clinical routine. An automated version (aBSI) has been developed and is now available. Multiple studies conducted across various clinical scenarios have demonstrated that aBSI plays a prognostic role, exhibiting correlations with overall survival (50).

In the context of breast cancer, MD Anderson criteria can be utilized to assess bone response (52). These criteria combine information from CT, MRI, radiography, and BS to classify the type of response. A prospective study based on MD Anderson criteria found a correlation between tumoral response at 6 months and progression-free survival (53).

In monitoring the treatment response of prostate cancer under ^{223}Ra therapy, the pivotal trial did not recommend specific radiological tests (54). Several retrospective studies reported an increase in the number of bone lesions on BS after 12 weeks in 21–28% of patients. However, only very few cases of confirmed progression were observed after six infusions, indicating the possibility of a flare phenomenon (55).

^{123}I-metaiodobenzylguanidine scintigraphy and bone metastases of neuroblastoma

Neuroblastoma is a common pediatric solid tumor originating from neural crest cells, which give rise to the adrenal medulla and sympathetic nervous system, expressing the norepinephrine transporter (56, 57). More than 50% of neuroblastomas are diagnosed at the metastatic stage (58), often involving bone and bone marrow (59), with only 30–40% long-term survival (60), necessitating more aggressive treatments (61). Therefore, imaging plays a crucial role in the initial staging and response assessment of neuroblastoma to guide therapeutic strategy.

mIBG is a norepinephrine analog taken up by neuroblastoma cells, allowing for the initial staging and response assessment of neuroblastoma, when labelled with ^{123}I, scintigraphic imaging. mIBG is excreted into the urinary tract, and its physiologic uptake includes salivary glands, liver, spleen, myocardium, lower to mid-lung zones, colon, brown fat, and uncommonly normal adrenal glands (62). No mIBG physiologic uptake is observed in bone or bone marrow, making it a good tracer to evaluate bone involvement in neuroblastoma (62). Concerning diagnostic performances of ^{123}I-mIBG planar scintigraphy in the detection of bone metastases, a 1988 study using histologic data as the gold standard found a sensitivity of 90% and a specificity of 100% (63). The addition of SPECT to planar scintigraphy is recommended, as it allows exact localization of uptake (i.e., bone versus soft-tissue uptake superimposed on planar acquisitions) and improves diagnostic accuracy (62, 64). However, mIBG imaging is time-consuming and suffers from poor spatial resolution compared to other current nuclear medicine modalities. Around 10% of neuroblastoma are not mIBG avid; in these cases, ^{18}F-FDG PET/CT is recommended (64). Furthermore, a recent systematic review reported better performances of PET imaging with catecholaminergic tracers than ^{123}I-mIBG in lesion-based analysis, notably for bone and bone marrow metastases, thanks to better sensitivity (65).

Several semi-quantitative scores have been developed to measure the extent of the disease and response to treatment. Two of them have shown good inter-observer concordance and a good correlation with outcome (66): SIOPEN score and Curie score, which should be used in initial and follow-up imaging (67). It is worth noting that the SIOPEN score only depends on the extent of bone involvement. More recent recommendations propose using the mIBG relative score (i.e., the absolute score of bone lesions at the time of response assessment divided by the absolute score of bone lesions at baseline before treatment) for response assessment (64).

Beyond the bone scan: positron emission tomography

^{18}F-NaF PET, the PET counterpart of BS

^{18}F-NaF is a PET bone tracer whose uptake mechanism resembles that of ^{99m}Tc-diphosphonates. In this process, ^{18}F substitutes for hydroxyl groups in hydroxyapatite and covalently bonds to the surface of new bone. Therefore, the level of ^{18}F-NaF uptake depends on both bone formation activity and loco-regional blood flow. Compared to ^{99m}Tc-diphosphonates, ^{18}F-NaF is characterized by faster pharmacokinetics, allowing image acquisition as soon as 30 min after injection, and a two-fold higher uptake in bone (68). Additionally, it benefits from the better spatial resolution and sensitivity of PET scanners compared to SPECT, providing a theoretically superior capacity to show smaller lesions.

Numerous studies and a few meta-analyses have assessed the diagnostic accuracy of ^{18}F-NaF PET/CT in detecting bone metastases from various primary tumors. In a 2019 meta-analysis on a patient-basis, Liu et al. reported various primaries pooled sensitivity of 93% (95% CI, 91–96%) and specificity of 95% (95% CI, 93–96%) when equivocal results were considered as negative, and 96% (95% CI, 93–97%) and 93% (95% CI, 91–55%) when equivocal results were considered as positive. They also included studies comparing ^{18}F-NaF

PET/CT to planar bone scintigraphy and found that ^{18}F-NaF PET/CT shows superior sensitivity and specificity when equivocal results were considered as positive, and superior sensitivity but no significant difference in specificity when equivocal results were considered as negative (69). Concerning prostate cancer specifically, Sheikhbahaei et al. also found excellent diagnostic performance, with a sensitivity of 98% (95% CI, 95–99%) and specificity of 90% (95% CI, 86–93%), surpassing ^{99m}Tc-diphosphonate SPECT +/− CT (AUC 0.996 versus 0.896, $p < 0.001$) (70). These results were reproduced in a recent prospective multicenter phase 3 trial comparing ^{18}F-NaF PET/CT to ^{99m}Tc-MDP SPECT/CT, including patients with breast or prostate cancer and a high risk or a clinical suspicion of bone involvement but without previous documented bone metastasis (71). Based on registry data, Hillner et al. have found that ^{18}F-NaF PET, with or without CT, have a significant impact on treatment management of prostate cancer in initial staging and follow-up (72). It should be noted, however, that this study did not make any comparison with bone scan data, making it impossible to compare the impact of the two modalities. This question was partially addressed in a 2019 study, where Zacho et al. found that ^{18}F-NaF PET/CT would provide no benefit in patients with a normal bone scan in initial staging (73). In an 81-patient population with moderate to high-risk prostate cancer, ^{18}F-NaF indicated bone metastasis in 1 patient and was equivocal in 7 patients, but all of them exhibited biochemical response after radical prostatectomy. On the other hand, a similar study performed in a situation of biochemical relapse after definitive therapy for localized prostate cancer and no relapse found on conventional imaging, including bone scan, found that ^{18}F-NaF PET/CT revealed bone metastases in 16% of the population, confirmed by clinical and imaging follow-up (74). However, it is noteworthy that ^{18}F-NaF PET/CT found suspicious bone uptake, disproven by follow-up, in 11% of the patients. ^{18}F-NaF PET/CT may, therefore, be able to detect bone metastases earlier, as suggested by another study reporting no difference between 18F-NaF PET/CT and BS for the response assessment of bone metastases from prostate cancer, perhaps due to a higher sensitivity at the baseline scan for ^{18}F-NaF PET/CT (75).

The quantification of ^{18}F-NaF uptake in bone metastases has been utilized in several studies to assess bone response (75–80). SUV_{max} is the main parameter used and has been shown to be correlated with PSA response, alkaline phosphatase kinetics, progression-free survival, and overall survival in prostate cancer (76, 78, 79), and to progression-free survival in breast cancer, using a threshold of ±25% change in SUVmax (81, 82). Similar to BS, ^{18}F-NaF PET/CT is also susceptible to the flare phenomenon, as described, for example in breast and prostate cancer (81, 83, 84).

^{18}F-FDG PET/CT for breast cancer management

^{18}F-FDG PET/CT has emerged as a cornerstone in oncology due to its ability to offer valuable insights into tumor metabolic activity. Acting as an analog of glucose, ^{18}F-FDG is transported from the blood to metabolically active cells, where it undergoes phosphorylation and, unlike glucose, is not further metabolized. The Warburg effect, which refers to cancer cells' heightened consumption of glucose compared to normal cells, leads to increased uptake of ^{18}F-FDG visible on PET imaging (85). Extensively used in oncology for cancer detection,

staging, and restaging, ^{18}F-FDG PET/CT enables clinicians to assess the effectiveness of ongoing treatments and identify potential disease recurrence. The ability to visualize metabolic changes before anatomical alterations occur enhances the sensitivity of the technique, contributing to early detection and intervention. Moreover, by gauging changes in metabolic activity post-therapy, clinicians can evaluate the effectiveness of treatments, allowing for timely adjustments to the therapeutic strategy. Various morphological and metabolic criteria have been proposed for this purpose, although they come with limitations in their application to bone metastases and in the context of the advent of targeted therapies and immunotherapy (86). Additionally, ^{18}F-FDG PET/CT assists in the localization of biopsy targets, guiding clinicians to areas with heightened metabolic activity for more accurate and informed tissue sampling. Beyond these clinical applications, ^{18}F-FDG PET/CT aids in the identification of distant metastases, contributing to a more comprehensive understanding of the disease's spread. Despite being a powerful tool, ^{18}F-FDG PET/CT has limitations, including false positives in areas of inflammation and false negatives in tumors with low glucose metabolism.

Initial staging

The shift toward using ^{18}F-FDG PET/CT instead of CT and BS in metastatic breast cancer staging (14), as recommended by the 2021 ESMO guidelines, aligns with numerous studies and meta-analyses comparing the diagnostic performances of these modalities. The *per-patient* sensitivities ranged from 81 to 93%, and the specificities ranged from 93 to 99%, with no significant differences noted between ^{18}F-FDG PET/CT and BS (17, 87, 88). However, it is worth noting that many patients were already undergoing treatment at the time of imaging, which can complicate definitive interpretations. Responding sclerotic metastases may show persistent radiotracer uptake on BS, even in the absence of ^{18}F-FDG uptake. A more recent study involving 84 patients with newly diagnosed metastatic breast cancer compared the performances of ^{18}F-FDG PET/CT and BS, revealing that ^{18}F-FDG PET/CT detected 87.4% of the total bone lesions, whereas BS identified only 26.3. Moreover, ^{18}F-FDG PET/CT led to clinically relevant management differences in 16% of patients compared to BS (89).

The immunohistochemical characteristics of breast cancers, such as estrogen receptor (ER), progesterone receptor (PR), HER2 receptor expression, and Ki67, play a crucial role in determining therapeutic options and are also correlated with tumor aggressiveness. This correlation extends to the degree of ^{18}F-FDG uptake, as confirmed by a recent meta-analysis. Tumors that are ER-negative, PR-negative, HER2-positive, and have a high Ki67 (>14%) exhibit significantly increased SUVmax (90). The histologic subtype of breast cancer further influences the level of ^{18}F-FDG uptake, with invasive ductal carcinoma (IDC) being more ^{18}F-FDG-avid than invasive lobular carcinoma (ILC) (91–93). Additionally, ILC bone metastases tend to be more often sclerotic than IDC metastases (91). Interestingly, BS appears to outperform ^{18}F-FDG PET/CT in detecting sclerotic metastases, with detection rates of 55.6–74% versus 95–100% for bone scintigraphy (Figure 2) (94, 95).

As previously indicated, ^{18}F-FDG PET/CT outperforms BS in the initial assessment not only of non-small cell lung carcinoma (23–25) but also in a variety of primitive such as renal carcinoma (96), hepatocellular carcinoma (97), head and neck cancers (98), or osteosarcoma (99).
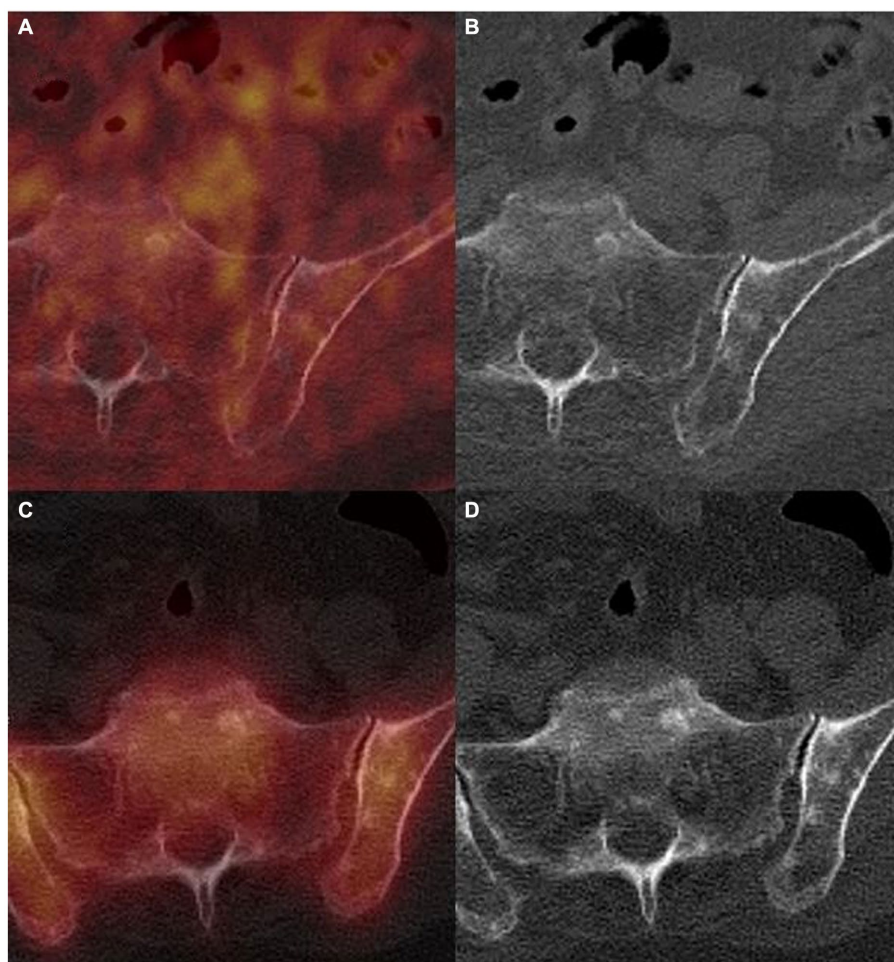
FIGURE 2
^{18}F-FDG PET/CT **(A,B)** and ^{99m}Tc-HMDP SPECT/CT **(C,D)** in a 75 years-old woman referred for initial staging of an invasive lobular carcinoma of the breast, showing multiples subcentimetric sclerotic bone lesions, linked to a diffuse bone invasion on the rest of the scans (not shown), without ^{18}F-FDG and ^{99m}Tc-HMDP uptake, corresponding to bone metastases confirmed by biopsy.

In the pre-therapeutic context, it is crucial to consider the histological subtype and immunohistochemical characteristics when encountering a consolidating bone lesion without ^{18}F-FDG uptake. For tumors with low ^{18}F-FDG avidity, the likelihood of a bone metastasis remains significant. It becomes important in such cases to search for other lesions with a similar phenotype that may exhibit uptake and to assess for morphologic progression based on previous imaging studies.

Response assessment

The efficacy of ^{18}F-FDG PET/CT in evaluating therapeutic bone responses has been investigated in studies involving patients with bone-only or bone-dominant metastatic breast cancer. There is a correlation between the evolution of tumoral uptake and the response assessed by changes in biological tumor markers, conventional imaging, and subjective symptoms in bone-dominant metastatic breast cancer (100). Furthermore, a retrospective study with 102 patients demonstrated that a decrease in ^{18}F-FDG uptake was an independent predictor of a longer response duration to treatment (101). These findings have been substantiated in recent studies (102, 103), indicating a significant correlation between higher uptake and shorter progression-free survival and shorter time before SRE occurs. Additionally, ^{18}F-FDG PET/CT appears capable of detecting a quantifiable measurable response earlier than CT in retrospective a series (104). In a prospective study, including 26% of patients with bone-only metastatic breast cancer, ^{18}F-FDG PET/CT identified disease progression 6 months earlier than CT did (105). Hence, ^{18}F-FDG PET/CT emerges as a reliable tool for assessing bone response to treatment, potentially influencing clinical therapeutic decisions compared to BS and CT. It is worth noting that a flare-up phenomenon has been reported within the first 7–10 days following the introduction of tamoxifen in a prospective trial evaluating the role of ^{18}F-FDG PET/CT in tamoxifen response assessment in breast cancer (106). However, this effect does not seem to persist over time, making it unlikely to be a source of misinterpretation. In the case of non-small cell lung cancer, a flare phenomenon has also been described in a series of four cases after 2 to 3 cycles (6 to 9 weeks) of bevacizumab associated with standard chemotherapy (107). It is worth noting that this effect did not involve non-osseous lesions.

Radiolabeled choline and PSMA PET/CT for prostate cancer management

Prostate cancer cells usually exhibit low avidity for ^{18}F-FDG, often showing no uptake on PET/CT scans. To address this limitation, two main radiotracers are available for molecular imaging of prostate cancer: radiolabeled choline and PSMA ligand (108, 109). Choline derivatives labeled with ^{18}F or ^{11}C are incorporated into phosphatidylcholine, a constituent of cell membranes, whose metabolism is increased in prostate cancer cells. PSMA, an enzyme highly expressed at the membranes of prostate cancer cells, serves as a target for radiolabeled PSMA ligands. These ligands bind to this enzyme and are subsequently internalized by the cell. Beyond its theragnostic potential via [177]-Lutetium (^{177}Lu)-PSMA, it has been demonstrated that this radiotracer is even more specific than radiolabeled choline, enabling the detection of millimetric or infraradiologic bone lesions.

Initial staging

Considering T-stage and N-stage, the less detailed anatomical information from CT (compared to MRI), the influence of the partial-volume effect, and the limited sensitivity for the detection of micro metastases appear to be the most significant drawbacks for accurate staging with choline PET/CT (108). Various studies have assessed ^{18}F-FCh PET/CT in the M staging of medium-to high-risk prostate cancer. Langsteger et al. reported a sensitivity and specificity of 91 and 83%, respectively, for the detection of bone metastases in prostate cancer patients (110). Wondergem et al. confirmed these favorable performances, reporting on a patient basis that sensitivity and specificity rates were 85.2 and 96.5% for ^{11}C-Choline and ^{18}F-FCh (111). It appears that ^{18}F-FCh PET/CT is more sensitive in the early

phase of the bone metastatic process, when the lesions are in the bone marrow and no cortical lesions are evident. In the clinical phase of the process, ^{18}F-FCh PET/CT and bone scintigraphy have similar diagnostic performances.

PSMA PET/CT also demonstrates excellent performance in the initial M staging of prostate cancer (Figure 3). An intriguing retrospective study involving 30 patients assessed the uptake of ^{68}Ga-PSMA-11 and the type of bone metastases (112). Surprisingly, the study revealed that radiotracer uptake was significantly higher in osteolytic and bone marrow metastases compared to osteoblastic ones. Among 126 patients who underwent PSMA PET and planar BS within 3 months, 37 patients were in the case of initial staging (113). In a patient-based analysis, the sensitivity and specificity were 100% (IC 95 76.8–100%) versus 71.4% (IC 95 41.9–91.6%), and 100% (IC 95 85.2–100%) versus 95.7% (IC 95 78.1–99.9%; $p = 0.006$) respectively. Hofman et al. recently published a prospective, randomized, multicenter study called proPSMA (114). Three hundred and two patients with high-risk prostate cancer were randomly assigned to conventional imaging (i.e., bone scintigraphy and computed tomography) or PSMA PET/CT for the initial staging. PSMA PET-CT had a 27% (95% IC 23–31%) greater accuracy than that of conventional imaging: 92% (95% IC 88–95%) versus 65% (95% IC 60–69%); $p < 0.0001$. Bone metastases were detected in 15/150 (10%) patients in the PSMA PET/CT group. Most interestingly, first-line conventional imaging conferred management change less frequently: 23% (95% IC 10–22%) versus 41% (95% IC 21–36%; $p = 0.008$).

Finally, one should be aware of the high rate of false-positive focal bone uptake with PSMA PET/CT, known as unspecific bone uptake (also known as UBU), whose etiology is still unknown. Several studies have reported a higher incidence with ^{18}F-F-PSMA than with ^{68}Ga-PSMA (115). Comparison with CT, other prostate-specific
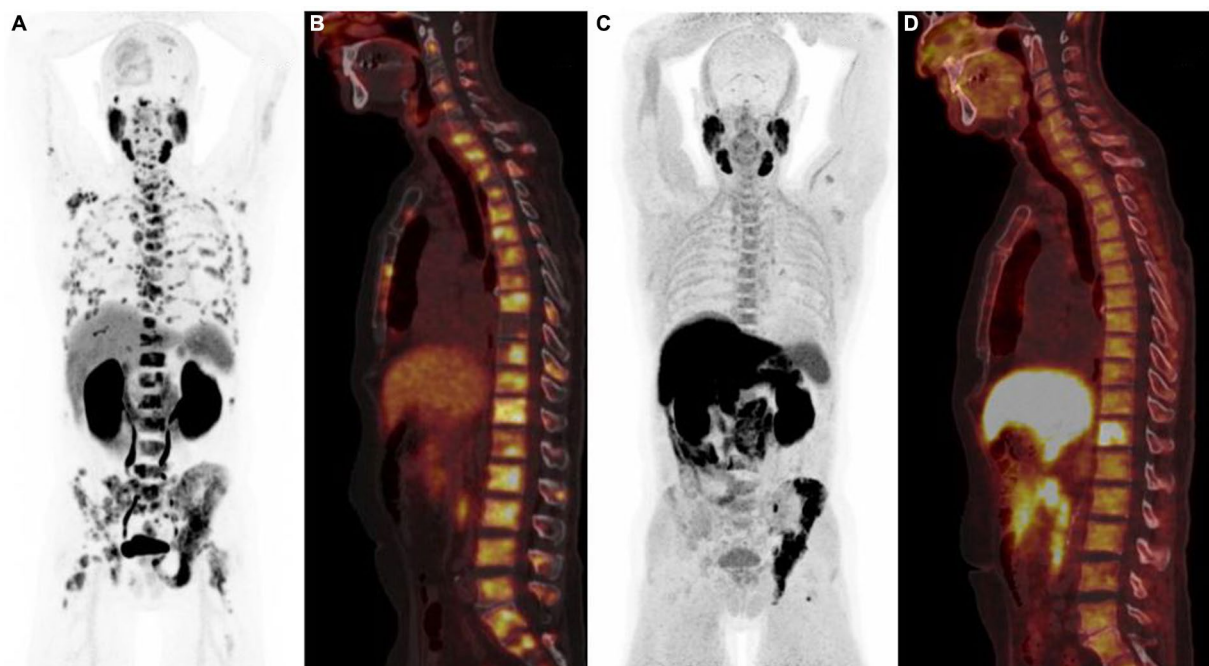

FIGURE 3
^{68}Ga-PSMA PET/CT [anterior MIP (A), sagittal PET/CT (B)] and ^{18}F-Fluorocholine PET/CT [anterior MIP (C), sagittal PET/CT (D)] illustrating the difference in sensitivity between the two radiotracers, ^{68}Ga-PSMA PET/CT showing more bone metastases than ^{18}F-Fluorocholine scan.

radiotracers, clinical history, and previous traumatic events is recommended to overcome this limitation (115).

Biochemical recurrence after a curative intent treatment

This stage of the disease is the most extensively studied for both choline and PSMA PET/CT. Fanti et al. published a meta-analysis of 18 articles with 2,126 patients evaluating the detection rate of ^{11}C-Choline PET/CT (116). The pooled detection rate, sensitivity, and specificity were 62% (95% IC 53–71%), 89% (95% IC 83–93%), and 89% (95% IC 73–96%) respectively. For bone metastases, eight studies with 775 participants reported detection rates. The pooled rate was 25% (95% IC 16–34%). Another meta-analysis focused on the detection of bone metastasis. Guo et al. analyzed 14 studies of 840 patients (117). On a per-patient analysis, the authors reported a pooled sensitivity, specificity, and negative likelihood ratio of 89% (95% CI 80–94%), 98% (95% CI 95–99%), and 12% (95% CI 7–20%) respectively. It is worth mentioning that despite its excellent performance for the detection of bone metastasis, a negative choline PET/CT cannot rule out the absence of bone lesions.

PSMA PET/CT has outperformed choline PET/CT in the diagnosis of biochemical relapse. A head-to-head comparison of ^{68}Ga-PSMA and ^{18}F-choline PET/CT was conducted on 37 patients (118). The detection rates were 86.5 and 70.3%, respectively, in favor of the PSMA PET/CT ($p = 0.04$). Schwenck et al. confirmed the superiority of PSMA PET/CT (versus ^{11}C-choline PET/CT) for the detection of both lymph nodes (94% versus 71%, $p < 0.001$) and bone metastases (98% versus 64%, $p < 0.001$) in this clinical setting (119). Moreover, it appears that the real benefit of PSMA PET/CT is in biological recurrences with low PSA levels. Burgard et al. retrospectively analyzed 115 patients with PSA levels under 0.2 ng/mL (120). Overall, 29 patients (25.2%) had lesions suspicious of prostate cancer. Eleven (25%) lesions out of 44 were bone metastases. Another recent meta-analysis confirmed these data (121). Thirty-seven articles with 4,790 patients were included. The authors reported that for PSA categories 0–0.19, 0.2–0.49, 0.5–0.99, 1–1.99, and ≥2 ng/mL, the percentages of positive scans were 33, 45, 59, 75, and 95%, respectively.

Of note, the performance of radiolabeled-choline PET/CT depends on both the PSA value at the time of the examination and the PSA doubling time (PSAdt). Castelluci et al. evaluated 605 patients treated with radical prostatectomy with an early biochemical relapse (PSA values between 0.2 ng/mL and 2 ng/mL; mean 1.05 ng/mL; median 1.07 ng/mL) (122). They reported an overall detection rate of 28.4% (172/605 patients). Bone lesions were observed in 56 patients (9.3%). The multivariate analysis confirmed that PSA value ($p = 0.011$) and PSA doubling time ($p < 0.001$) were significant predictors of PET/CT positivity, with optimal cutoff values of 1.05 ng/mL and 5.95 months. This also concerns the ligand PET/CT. A retrospective analysis of 1,007 patients who underwent ^{68}Ga-PSMA PET/CT reported an overall detection rate of 79.5% (801 patients) (123), with 131 (13%) patients diagnosed with bone metastases. The authors confirmed that PSA level was significantly associated with a pathological PET/CT result ($p < 0.001$).

Therapy response assessment

A very few studies have evaluated choline PET/CT for the therapy response assessment of castration-resistant prostate cancer, whether with chemotherapy or hormone therapy. Schwarzenböck et al.

monitored 11 patients treated with docetaxel (124), De Giorgi et al. evaluated 43 patients under abiraterone (69), and 36 patients under enzalutamide (70). These studies reported a high percentage of discrepancy between PSA and PET/CT results and did not provide many details on the evolution of bone metastases under treatment.

On the other hand, there is rapidly growing evidence that promises a place for PSMA PET/CT in this indication. The first step was to create an international framework for response evaluation criteria. The question is not fully resolved yet, with several classifications already in use: the adapted PCWG3 (using PSMA PET instead of bone scan), the PSMA PET Progression criteria (PPP) (125), and the RECIP 1.0 classification (126). Gafita et al. compared all those criteria in 124 men with a metastatic RCPC (127) and demonstrated that the RECIP 1.0 classification was the most correlated to patient outcomes.

As already explained, PCWG3 defines bone progression as the appearance of at least 2 new lesions (with two or more additional new lesions on a confirmatory scan, 2 + 2 rule). In contrast, because of its high specificity, 1 new distant lesion by PSMA PET is considered progressive disease by PPP if the following criteria are met: consistent clinical or laboratory data, including PSA and other parameters such as pain assessment, lactate dehydrogenase, and anemia (125). The RECIP 1.0 criteria mainly focus on the PSMA uptake volume for therapy response assessment under ^{177}Lu-PSMA therapy (126). The definition of a new lesion is as follows: the appearance of at least 1 new PSMA-positive lesion, defined as any new focal uptake of PSMA ligand higher than the surrounding background. The authors recognized that there was no external validation of their threshold definition and that they could not compare the prognostic ability of RECIP versus PCWG3 criteria, since bone scans were not included in the clinical workup of ^{177}Lu-PSMA radionuclide therapy at all institutions.

One prospective trial studied the role of PSMA PET/CT in the follow-up of [223]Ra therapy and showed progressive bone disease in 89% of the patients, with the overall burden of disease on PSMA being strongly correlated with PSA changes (128). Since PSA seems inappropriate for evaluating the response to [223]Ra therapy (128, 129), the role of PSMA PET/CT for monitoring patients under [223]Ra appears limited.

Focusing on bone metastases, Schmidkonz et al. investigated 177 men suffering from 443 bone lesions on ^{68}Ga-PSMA-11 PET (130). Within this cohort, 20 patients with 173 bone metastases underwent PSMA PET/CT imaging before and after therapies. Bone metastases showed a mean density of 589 ± 203 HU before therapy, with a significant increase to 827 ± 215 HU ($p < 0.05$). None of the other CT-derived parameters had significant changes under therapies. In contrast, a significant correlation was observed between the percentage differences of whole-body total metabolic volume and the percentage difference of serum-PSA levels ($p < 0.001$) before and after therapies. The main limitation was the vast heterogeneity of treatments used (radiation therapy, androgen deprivation therapy, chemotherapy, and radioligand therapy).

The flare phenomenon has also been described in several case reports and studies between 2 and 6 weeks following treatment initiation, depending on study design (131–133). It is not exactly known how long a flare-up can be observed on PSMA PET/CT, but it is worth noting that one study described no flare phenomenon after a median follow-up of 3 months in 26 patients (134).

^{18}F-FDOPA and ^{68}Ga-DOTA-peptides PET/CT for neuroendocrine tumors management

Neuroendocrine tumors (NETs) are rare and heterogeneous epithelial neoplasms with neuroendocrine differentiation. The primary site of origin for NETs, accounting for approximately 60% of cases, is the gastrointestinal (GI) tract, with the small intestine being the foremost location of tumor development (135, 136). The incidence of bone metastases in patients with NETs has been investigated mainly through retrospective studies. Data from US institutional registries indicate that around 12% of patients with NETs develop bone metastatic disease (137, 138). This finding aligns with the results of a recent European study, which examined 677 patients diagnosed with NETs from 2000 to 2015 (139). Generally, bone metastases in NETs appear to be more frequent in lung carcinoids compared to gastroenteropancreatic neuroendocrine tumors (GEP-NETs). Among GEP-NETs, rectal NETs consistently exhibit the highest propensity for metastasizing to the bones (140).

While bone involvement is incidentally discovered in as many as 40% of NET patients, clinical complications arising from bone metastases have been noted in roughly half of these cases (138). Typically, NET bone metastases affect the axial skeleton more frequently than the appendicular bones, and identifying radiographic signs can be challenging. When standard radiography and CT scans are employed, NET bone metastases tend to exhibit either an osteosclerotic pattern or a combination of osteolytic and osteosclerotic features. It seems that MRI exhibits higher sensitivity in the detection of NET bone lesions compared to CT. Whole-body MRI with diffusion-weighted imaging, in particular, is noted for its substantial diagnostic accuracy in this regard (141–144).

The prognosis for NET patients with bone metastases varies widely based on factors such as the extent of bone involvement, the aggressiveness of the primary tumor, and the effectiveness of treatment. While bone metastases in NETs are generally associated with a more indolent course compared to some other cancers, they can still significantly impact a patient's quality of life and overall survival. Evidence indicates that NET patients diagnosed with synchronous bone metastases tend to experience less favorable survival outcomes when compared to those with metachronous bone metastases that appear later after diagnosis (145, 146). Interestingly, the impact of bone metastases on survival appears to be more significant in patients with pancreatic NETs than with intestinal NETs (147). Notably, in lung NETs, the presence of bone metastases is associated with a poor prognosis, regardless of the tumor grade or whether the metastases occur synchronously or metachronously (141).

Over the last 20 years, nuclear medicine imaging methods for NETs have undergone gradual advancements (148, 149). The introduction of radiotracers such as ^{18}F-Fluoro-dihydroxyphenylalanine (^{18}F-DOPA) and ^{68}Ga-DOTA-peptides for PET imaging has revolutionized the diagnosis and management of NETs. These cutting-edge tools provide unprecedented insights into localization, characterization, and treatment planning, elevating the precision of care for patients grappling with these complex malignancies (150).

Due to the moderate-to-high overexpression of somatostatin receptors (SSTR), predominantly subtype 2A, the primary imaging technique for diagnosis and assessment involves SSTR imaging. Synthetic somatostatin analogs (SSAs), such as octreotide, have been effectively labeled for medical imaging. Among these radiopharmaceuticals, ^{111}In-pentetreotide (OctreoScan) has demonstrated its utility for gamma camera studies over more than two decades. Recently, a new category of somatostatin analogs, labeled with the positron-emitting radionuclide ^{68}Ga for PET/CT imaging and called ^{68}Ga-DOTA-peptides (^{68}Ga-DOTATOC, ^{68}Ga-DOTATATE, and ^{68}Ga-DOTANOC), has emerged as the current gold standard for assessing NETs (148, 149). The introduction of ^{68}Ga-DOTA-peptide PET/CT has significantly improved the detection of skeletal metastases, surpassing both bone scintigraphy and OctreoScan scintigraphy in performance. Recent studies indicate that ^{68}Ga-DOTA-peptide PET/CT demonstrates a diagnostic accuracy ranging from 80 to 100% in identifying NET bone lesions (151–154). When compared to contrast-enhanced CT and MRI, ^{68}Ga-DOTA-peptide PET/CT may enhance diagnostic capabilities by approximately 20 to 25% in the detection of bone metastases (Figure 4) (151, 152, 155, 156).

Peptide Receptor Radionuclide Therapy (PRRT) is a targeted therapeutic approach for NETs involving the administration of a radiolabeled somatostatin analog, typically ^{177}Lu. This analog specifically binds to somatostatin receptors overexpressed in NETs, leading to the selective delivery of beta particle-emitting radiation and localized cytotoxic effects. PRRT has demonstrated efficacy in controlling tumor progression, especially in metastatic scenarios where conventional treatment modalities may be limited (157). As a personalized and targeted therapeutic strategy, PRRT holds promise in optimizing outcomes and managing symptoms associated with NETs. Post-treatment SPECT/CT imaging after PRRT is critical for dosimetric evaluation (158) and is potentially useful for monitoring treatment efficacy and promptly detecting disease progression during treatment. However, no studies have specifically focused on the efficacy of post-PRRT SPECT/CT imaging for bone metastases monitoring. On the other hand, ^{68}Ga-DOTA-peptide PET/CT has been successfully used to monitor PRRT efficacy in patients with bone metastases of NETs treated by ^{177}Lu-DOTA-octreotate. The treatment results in prolonged overall survival and provides relief from pain, supporting the consideration of PRRT in the management of advanced bone metastatic disease (159, 160).

Importantly, non-tumoral processes with elevated osteoblastic activity can also present challenges in the interpretation of ^{68}Ga-DOTA-peptides PET, as they may exhibit increased osseous uptake. These situations encompass a range of conditions, including degenerative alterations, fractures, and non-malignant lesions like hemangioma, enchondroma, and fibrous dysplasia. Additionally, meningiomas, often incidentally discovered, manifest as intensely avid masses located outside the brain parenchyma. They are typically found along the cerebral convexity, in the parasagittal region, or originating from the sphenoid wing (161).

In addition to ^{68}Ga-DOTA-peptides, ^{18}F-DOPA has been successfully proposed for *in vivo* nuclear imaging of NETs (162, 163). The heightened uptake of ^{18}F-DOPA in NETs results from increased cellular synthesis, storage, and secretion of biogenic amines. As a result, the sensitivity of ^{18}F-DOPA PET is influenced by the NET's embryological origin and differentiation. Specific tumoral features, such as the biosynthesis of serotonin, play a significant role in explaining the superior sensitivity of ^{18}F-DOPA PET for small intestine carcinoids (SiNET). ^{18}F-FDOPA PET outperforms morphological imaging (CT) and gamma camera-based SSTR imaging for the detection of skeletal metastases, lymph nodes, and liver lesions in patients with low-grade midgut NETs. The sensitivity of ^{18}F-FDOPA PET was 100, 95, and 96% respectively, in per patient, per region, and per lesion analysis (164). Becherer et al. reported sensitivities of 90.9% for the skeleton in the evaluation of patients with histologically proven NETs (165). In a recent study by Deleval et al., ^{18}F-DOPA PET/CT detected bone metastases in 46 of 155 (29.7%) SiNET patients, with a
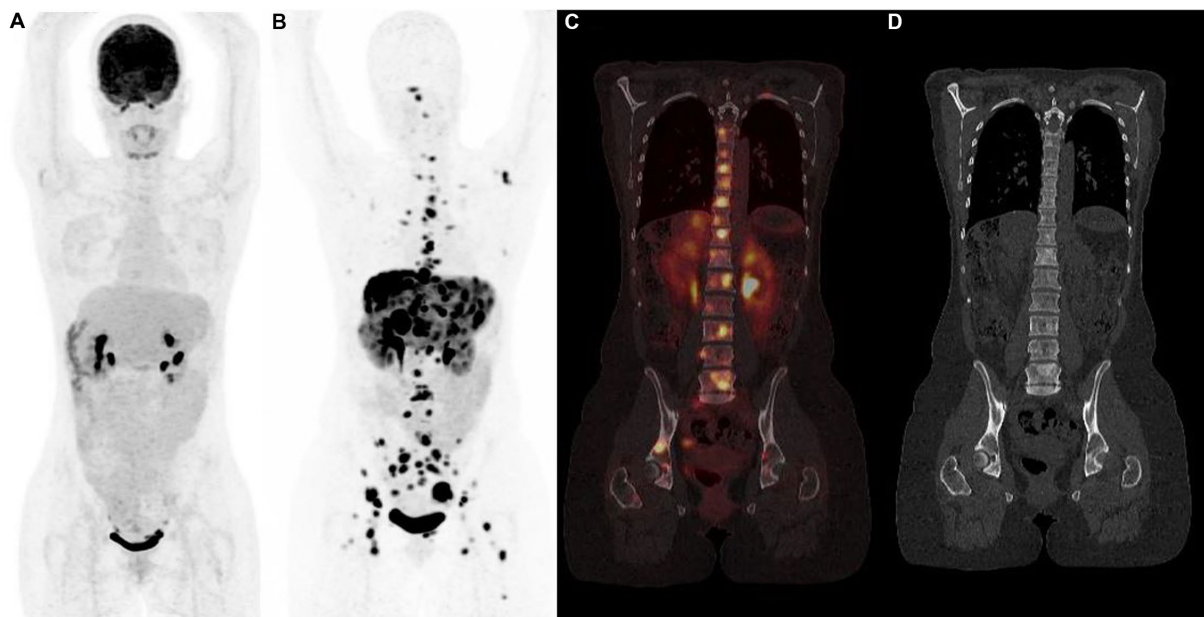
FIGURE 4
^{18}F-FDG (A) and ^{68}Ga-DOTATOC (B–D) PET/CT results (anterior MIP, coronal PET/CT, coronal CT) in a 48 years-old woman with grade 2 metastatic pancreatic neuroendocrine tumor showing multiple bone sclerotic metastases characterized by intense and pathologic ^{68}Ga-DOTATOC uptake. ^{18}F-FDG PET/CT failed to detect metastatic spread.
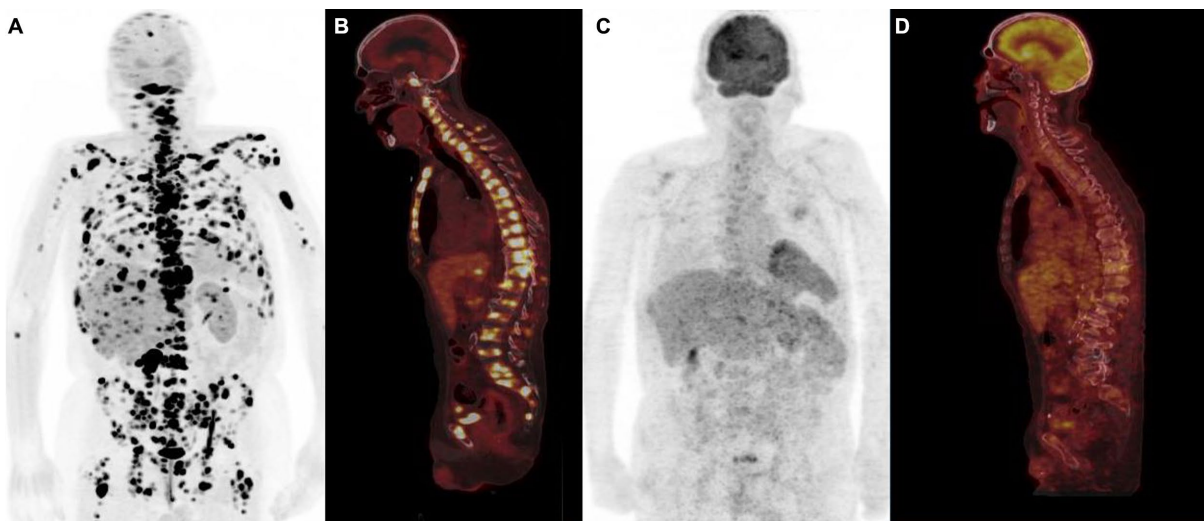

FIGURE 5
Typical example of "flip-flop" effect (anterior PET MIP, sagittal PET/CT) in a patient with metastatic low-grade (G1) small bowel NET. 18F-FDOPA PET showed multiple sclerotic bone metastases (A,B) not detectable by 18F-FDG PET (C,D), emphasizing the role of tumor grade in the selection of the optimal diagnostic radiotracer.

negative prognostic impact (166). In a recent ^{18}F-DOPA PET/CT study, Lelièvre et al. (167) described the topographical distribution of bone metastases in patients with SiNET, mainly involving the spine, pelvic bones, and ribs. Metabolic tumor volume (MTV), excluding bone lesions, greater than 19.2 mL, and hepatic metastatic involvement were significant predictors of bone metastases.

More recently, several retrospective studies (168–171) and one systematic review (172) have compared ^{18}F-FDOPA PET/CT and SSTR PET/CT in well-differentiated small intestine NETs. Despite similar high patient-and region-based pooled sensitivities (83 and

89%, respectively, for ^{18}F-DOPA PET; 88 and 92%, respectively, for SSTR PET), ^{18}F-DOPA demonstrated superiority in lesion detection (lesion-based pooled sensitivity, 95% vs. 82%). This higher diagnostic performance was also observed in the case of bone metastases (168, 169). Specifically, ^{18}F-DOPA PET/CT exhibited greater sensitivity than ^{68}Ga-DOTA peptides PET/CT in patients with high levels of serotonin and 5-hydroxyindoleacetic acid (169, 170).

The limited value of ^{18}F-FDG PET/CT is typically reported in the management of low-grade NETs, likely due to their low metabolic activity and slow growth (Figure 5). Despite these considerations,

^{18}F-FDG PET holds potential for prognostic stratification in patients with NETs. Notably, NETs exhibiting increased ^{18}F-FDG uptake tend to display more aggressive behavior, leading to a less favorable long-term prognosis ([173]).

Conclusion

Despite their widespread use in staging and assessing bone metastases, BS have limitations impacting sensitivity and specificity, particularly in the follow-up of patients undergoing therapy. PET/CT has effectively addressed these limitations, demonstrating potential therapeutic impact, as seen in breast cancer. Nuclear bone imaging is now evolving towards the use of more specific PET tracers tailored to each tumor type, a trend already established for prostate and neuroendocrine tumors. Additionally, the advent of large field-of-view PET/CT, enabling dynamic imaging of extensive portions of the body, should have an interest in response assessment of bone metastases. Finally, PET/MR devices may contribute to enhancing diagnostic performance by leveraging complementary information from both modalities.

Author contributions

EO: Supervision, Validation, Writing – original draft, Writing – review & editing. AK: Writing – review & editing. NP: Writing – review & editing. CP: Writing – review & editing. FS: Writing – review & editing, Writing – original draft. AI: Writing – original draft, Writing – review & editing.

Conflict of interest

The authors declare that the research was conducted in the absence of any commercial or financial relationships that could be construed as a potential conflict of interest.

Publisher's note

All claims expressed in this article are solely those of the authors and do not necessarily represent those of their affiliated organizations, or those of the publisher, the editors and the reviewers. Any product that may be evaluated in this article, or claim that may be made by its manufacturer, is not guaranteed or endorsed by the publisher.

References

1. Coleman RE. Clinical features of metastatic bone disease and risk of skeletal morbidity. *Clin Cancer Res Off J Am Assoc Cancer Res.* (2006) 12:6243s–9s. doi: 10.1158/1078-0432.CCR-06-0931

2. D'Oronzo S, Coleman R, Brown J, Silvestris F. Metastatic bone disease: pathogenesis and therapeutic options: up-date on bone metastasis management. *J Bone Oncol.* (2019) 15:100205–004. doi: 10.1016/j.jbo.2018.10.004

3. Bruyn D. Structural substrates of bone marrow function. *Semin Hematol.* (1981) 18:179–93.

4. Goltzman D. Mechanisms of the development of osteoblastic metastases. *Cancer.* (1997) 80:1581–7. doi: 10.1002/(SICI)1097-0142(19971015)80:8+<1581::AID-CNCR8>3.0.CO;2-N

5. Paget S. The distribution of secondary growths in cancer of the breast. 1889. *Cancer Metastasis Rev.* (1989) 8:98–101.

6. Mundy GR. Mechanisms of bone metastasis. *Cancer.* (1997) 80:1546–56. doi: 10.1002/(SICI)1097-0142(19971015)80:8+<1546::AID-CNCR4>3.0.CO;2-I

7. Clézardin P, Coleman R, Puppo M, Ottewell P, Bonnelye E, Paycha F. Bone metastasis: mechanisms, therapies, and biomarkers. *Physiol Rev.* (2021) 101:797–855. doi: 10.1152/physrev.00012.2019

8. Cook GJR, Goh V. Molecular imaging of bone metastases and their response to therapy. *J Nucl Med Off Publ Soc Nucl Med.* (2020) 61:799–806. doi: 10.2967/jnumed.119.234260

9. Vaz S, Usmani S, Gnanasegaran G, Van den Wyngaert T. Molecular imaging of bone metastases using bone targeted tracers. *Q J Nucl Med Mol Imaging Off Publ Ital Assoc Nucl Med AIMN.* (2019) 63:112–28. doi: 10.23736/S1824-4785.19.03198-4

10. Cook GJ, Goh V. Functional and hybrid imaging of bone metastases. *J Bone Miner Res Off J Am Soc Bone Miner Res.* (2018) 33:961–72. doi: 10.1002/jbmr.3444

11. Einhorn TA, Vigorita VJ, Aaron A. Localization of technetium-99m methylene diphosphonate in bone using microautoradiography. *J Orthop Res Off Publ Orthop Res Soc.* (1986) 4:180–7. doi: 10.1002/jor.1100040206

12. Silberstein EB, Saenger EL, Tofe AJ, Alexander GW, Park HM. Imaging of bone metastases with 99m Tc-Sn-EHDP (diphosphonate), 18 F, and skeletal radiography. *Radiology.* (1973) 107:551–5. doi: 10.1148/107.3.551

13. Love C, Din AS, Tomas MB, Kalapparambath TP, Palestro CJ. Radionuclide bone imaging: an illustrative review. *Radiogr Rev Publ Radiol Soc N Am Inc.* (2003) 23:341–58. doi: 10.1148/rg.232025103

14. Gennari A, André F, Barrios CH, Cortés J, de Azambuja E, DeMichele A. ESMO clinical practice guideline for the diagnosis, staging and treatment of patients with metastatic breast cancer. *Ann Oncol Off J Eur Soc Med Oncol.* (2021) 32:1475–95. doi: 10.1016/j.annonc.2021.09.019

15. Trabulsi EJ, Rumble RB, Jadvar H, Hope T, Pomper M, Turkbey B. Optimum imaging strategies for advanced prostate Cancer: ASCO guideline. *J Clin Oncol Off J Am Soc Clin Oncol.* (2020) 38:1963–96. doi: 10.1200/JCO.19.02757

16. Parker C, Castro E, Fizazi K, Heidenreich A, Ost P. Prostate cancer: ESMO clinical practice guidelines for diagnosis, treatment and follow-up. *Ann Oncol Off J Eur Soc Med Oncol.* (2020) 31:1119–34. doi: 10.1016/j.annonc.2020.06.011

17. Shie P, Cardarelli R, Brandon D, Erdman W, Abdulrahim N. Meta-analysis: comparison of F-18 fluorodeoxyglucose-positron emission tomography and bone scintigraphy in the detection of bone metastases in patients with breast cancer. *Clin Nucl Med.* (2008) 33:97–101. doi: 10.1097/RLU.0b013e31815f23b7

18. Sugihara T, Koizumi M, Koyama M, Terauchi T, Gomi N. Bone metastases from breast cancer: associations between morphologic CT patterns and glycolytic activity on PET and bone scintigraphy as well as explorative search for influential factors. *Ann Nucl Med.* (2017) 31:719–25. doi: 10.1007/s12149-017-1202-3

19. Hansen JA, Naghavi-Behzad M, Gerke O, Baun C, Falch K, Duvnjak S. Diagnosis of bone metastases in breast cancer: lesion-based sensitivity of dual-time-point FDG-PET/CT compared to low-dose CT and bone scintigraphy. *PLoS One.* (2021) 16:e0260066. doi: 10.1371/journal.pone.0260066

20. Sohaib SA, Cook G, Allen SD, Hughes M, Eisen T, Gore M. Comparison of whole-body MRI and bone scintigraphy in the detection of bone metastases in renal cancer. *Br J Radiol.* (2009) 82:632–9. doi: 10.1259/bjr/52773262

21. Staudenherz A, Steiner B, Puig S, Kainberger F, Leitha T. Is there a diagnostic role for bone scanning of patients with a high pretest probability for metastatic renal cell carcinoma? *Cancer.* (1999) 85:153–5. doi: 10.1002/(SICI)1097-0142(19990101)85:1<153::AID-CNCR21>3.0.CO;2-#

22. Wu HC, Yen RF, Shen YY, Kao CH, Lin CC, Lee CC. Comparing whole body 18F-2-deoxyglucose positron emission tomography and technetium-99m methylene diphosphate bone scan to detect bone metastases in patients with renal cell carcinomas - a preliminary report. *J Cancer Res Clin Oncol.* (2002) 128:503–6. doi: 10.1007/s00432-002-0370-1

23. Chang MC, Chen JH, Liang JA, Lin CC, Yang KT. Meta-analysis: comparison of F-18 fluorodeoxyglucose-positron emission tomography and bone scintigraphy in the

detection of bone metastasis in patients with lung cancer. *Acad Radiol.* (2012) 19:349–57. doi: 10.1016/j.acra.2011.10.018

24. Liu T, Xu JY, Xu W, Bai YR, Yan WL, Yang HL. Fluorine-18 deoxyglucose positron emission tomography, magnetic resonance imaging and bone scintigraphy for the diagnosis of bone metastases in patients with lung cancer: which one is the best? – a meta-analysis. *Clin Oncol R Coll Radiol G B.* (2011) 23:350–8. doi: 10.1016/j.clon.2010.10.002

25. Qu X, Huang X, Yan W, Wu L, Dai K. A meta-analysis of [18]FDG-PET-CT, [18]FDG-PET, MRI and bone scintigraphy for diagnosis of bone metastases in patients with lung cancer. *Eur J Radiol.* (2012) 81:1007–15. doi: 10.1016/j.ejrad.2011.01.126

26. Chow KM, So WZ, Lee HJ, Lee A, Yap DWT, Takwoingi Y. Head-to-head comparison of the diagnostic accuracy of prostate-specific membrane antigen positron emission tomography and conventional imaging modalities for initial staging of intermediate-to high-risk prostate Cancer: a systematic review and Meta-analysis. *Eur Urol.* (2023) 84:36–48. doi: 10.1016/j.eururo.2023.03.001

27. Lecouvet FE, Talbot JN, Messiou C, Bourguet P, Liu Y. Monitoring the response of bone metastases to treatment with magnetic resonance imaging and nuclear medicine techniques: a review and position statement by the European Organisation for Research and Treatment of Cancer imaging group. *Eur J Cancer Oxf Engl.* (1990) 50:2519–31. doi: 10.1016/j.ejca.2014.07.002

28. Woolf DK, Padhani AR, Makris A. Assessing response to treatment of bone metastases from breast cancer: what should be the standard of care? *Ann Oncol Off J Eur Soc Med Oncol.* (2015) 26:1048–57. doi: 10.1093/annonc/mdu558

29. Iuliani M, Pantano F, Buttigliero C, Fioramonti M, Bertaglia V. Biological and clinical effects of abiraterone on anti-resorptive and anabolic activity in bone microenvironment. *Oncotarget.* (2015) 6:12520–8. doi: 10.18632/oncotarget.3724

30. Stokkel MP, Valdés Olmos RA, Hoefnagel CA, Richel DJ. Tumor and therapy associated abnormal changes on bone scintigraphy. Old and new phenomena. *Clin Nucl Med.* (1993) 18:821–8. doi: 10.1097/00003072-199310000-00001

31. Singh V, Dikshit S, Ora M, Nazar AH. Metabolic flare phenomenon mimicking disease progression on 18Flouride- Fluorodeoxyglucose PET/CT scan in breast cancer treated with paclitaxel-based chemotherapy. *Asia Ocean J Nucl Med Biol.* (2023) 11:175–80. doi: 10.22038/AOJNMB.2022.68237.1474

32. Malaspina S, Ettala O, Tolvanen T, Rajander J, Eskola O. Flare on [18F]PSMA-1007 PET/CT after short-term androgen deprivation therapy and its correlation to FDG uptake: possible marker of tumor aggressiveness in treatment-naïve metastatic prostate cancer patients. *Eur J Nucl Med Mol Imaging.* (2023) 50:613–21. doi: 10.1007/s00259-022-05970-y

33. Weisman AJ, Harmon SA, Perk TG, Eickhoff J, Choyke PL, Kurdziel KA. Quantification of bone flare on 18F-NaF PET/CT in metastatic castration-resistant prostate cancer. *Prostate Cancer Prostatic Dis.* (2019) 22:324–30. doi: 10.1038/s41391-018-0110-5

34. Chao HS, Chang CP, Chiu CH, Chu LS, Chen YM. Bone scan flare phenomenon in non-small-cell lung cancer patients treated with gefitinib. *Clin Nucl Med.* (2009) 34:346–9. doi: 10.1097/RLU.0b013e3181a344df

35. Scher HI, Morris MJ, Stadler WM, Higano C, Basch E, Fizazi K. Trial design and objectives for castration-resistant prostate Cancer: updated recommendations from the prostate Cancer clinical trials working group 3. *J Clin Oncol Off J Am Soc Clin Oncol.* (2016) 34:1402–18. doi: 10.1200/JCO.2015.64.2702

36. Messiou C, Cook G, Reid AHM, Attard G, Dearnaley D. The CT flare response of metastatic bone disease in prostate cancer. *Acta Radiol Stockh Swed 1987.* (2011) 52:557–61. doi: 10.1258/ar.2011.100342

37. Cook GJR, Venkitaraman R, Sohaib AS, Lewington VJ, Chua SC. The diagnostic utility of the flare phenomenon on bone scintigraphy in staging prostate cancer. *Eur J Nucl Med Mol Imaging.* (2011) 38:7–13. doi: 10.1007/s00259-010-1576-0

38. Kesler M, Druckmann I, Levine C, Kuten J, Yossepowitch O. 68Ga-PSMA-11 PET/CT follow-up of patients with prostate Cancer with bone metastases who had reduced bone density after androgen deprivation therapy. *Diagn Basel Switz.* (2021) 11:277. doi: 10.3390/diagnostics11020277

39. Pollen JJ, Reznek RH, Talner LB. Lysis of osteoblastic lesions in prostatic cancer: a sign of progression. *AJR Am J Roentgenol.* (1984) 142:1175–9. doi: 10.2214/ajr.142.6.1175

40. DeMeo JH, Balseiro J, Cole TJ. Etidronate sodium therapy – a cause of poor skeletal radiopharmaceutical uptake. *Semin Nucl Med.* (1991) 21:332. doi: 10.1016/S0001-2998(05)80136-9

41. Hommeyer SH, Varney DM, Eary JF. Skeletal nonvisualization in a bone scan secondary to intravenous etidronate therapy. *J Nucl Med Off Publ Soc Nucl Med.* (1992) 33:748–50.

42. Sandler ED, Parisi MT, Hattner RS. Duration of etidronate effect demonstrated by serial bone scintigraphy. *J Nucl Med Off Publ Soc Nucl Med.* (1991) 32:1782–4.

43. Krasnow AZ, Collier BD, Isitman AT, Hellman RS, Ewey D. False-negative bone imaging due to etidronate disodium therapy. *Clin Nucl Med.* (1988) 13:264–7. doi: 10.1097/00003072-198804000-00008

44. Pecherstorfer M, Schilling T, Janisch S, Woloszczuk W, Baumgartner G. Effect of clodronate treatment on bone scintigraphy in metastatic breast cancer. *J Nucl Med Off Publ Soc Nucl Med.* (1993) 34:1039–44.

45. Morris PG, Poznak CV, Modi S, Mak AF, Patil S. Intravenous bisphosphonate therapy does not acutely alter nuclear bone scan results. *Clin Breast Cancer.* (2010) 10:33–9. doi: 10.3816/CBC.2010.n.004

46. Carrasquillo JA, Whatley M, Dyer V, Figg WD, Dahut W. Alendronate does not interfere with 99mTc-methylene diphosphonate bone scanning. *J Nucl Med Off Publ Soc Nucl Med.* (2001) 42:1359–63.

47. Roudier MP, Vesselle H, True LD, Higano CS, Ott SM. Bone histology at autopsy and matched bone scintigraphy findings in patients with hormone refractory prostate cancer: the effect of bisphosphonate therapy on bone scintigraphy results. *Clin Exp Metastasis.* (2003) 20:171–80. doi: 10.1023/A:1022627421000

48. Wong KK, Piert M. Dynamic bone imaging with 99mTc-labeled diphosphonates and 18F-NaF: mechanisms and applications. *J Nucl Med Off Publ Soc Nucl Med.* (2013) 54:590–9. doi: 10.2967/jnumed.112.114298

49. Fushimi M, Ohbayashi Y, Nakai F, Norikane T, Yamamoto Y. The effect of zoledronic acid and denosumab on the mandible and other bones: a 18F-NaF-PET study. *Oral Radiol.* (2022) 38:594–600. doi: 10.1007/s11282-022-00594-2

50. Mota JM, Armstrong AJ, Larson SM, Fox JJ, Morris MJ. Measuring the unmeasurable: automated bone scan index as a quantitative endpoint in prostate cancer clinical trials. *Prostate Cancer Prostatic Dis.* (2019) 22:522–30. doi: 10.1038/s41391-019-0151-4

51. Imbriaco M, Larson SM, Yeung HW, Mawlawi OR, Erdi Y. A new parameter for measuring metastatic bone involvement by prostate cancer: the bone scan index. *Clin Cancer Res Off J Am Assoc Cancer Res.* (1998) 4:1765–72.

52. Hamaoka T, Madewell JE, Podoloff DA, Hortobagyi GN, Ueno NT. Bone imaging in metastatic breast cancer. *J Clin Oncol Off J Am Soc Clin Oncol.* (2004) 22:2942–53. doi: 10.1200/JCO.2004.08.181

53. Hayashi N, Costelloe CM, Hamaoka T, Wei C, Niikura N. A prospective study of bone tumor response assessment in metastatic breast cancer. *Clin Breast Cancer.* (2013) 13:24–30. doi: 10.1016/j.clbc.2012.09.004

54. Parker C, Nilsson S, Heinrich D, Helle SI, O'Sullivan JM, Fosså SD. Alpha emitter radium-223 and survival in metastatic prostate cancer. *N Engl J Med.* (2013) 369:213–23. doi: 10.1056/NEJMoa1213755

55. Rodriguez-Vida A, Torregrosa MD, Pinto Á, Climent MÁ, Olmos D. Selection and monitoring of patients with metastatic castration-resistant prostate cancer for treatment with radium-223. *Clin Transl Oncol Off Publ Fed Span Oncol Soc Natl Cancer Inst Mex.* (2018) 20:679–86. doi: 10.1007/s12094-017-1785-0

56. Pfluger T, Piccardo A. Neuroblastoma: MIBG imaging and new tracers. *Semin Nucl Med.* (2017) 47:143–57. doi: 10.1053/j.semnuclmed.2016.10.007

57. Olecki E, Grant CN. MIBG in neuroblastoma diagnosis and treatment. *Semin Pediatr Surg.* (2019) 28:150859. doi: 10.1016/j.sempedsurg.2019.150859

58. Maris JM, Hogarty MD, Bagatell R, Cohn SL. Neuroblastoma. *Lancet Lond Engl.* (2007) 369:2106–20. doi: 10.1016/S0140-6736(07)60983-0

59. DuBois SG, Kalika Y, Lukens JN, Brodeur GM, Seeger RC. Metastatic sites in stage IV and IVS neuroblastoma correlate with age, tumor biology, and survival. *J Pediatr Hematol Oncol.* (1999) 21:181–9. doi: 10.1097/00043426-199905000-00005

60. Park JR, Eggert A, Caron H. Neuroblastoma: biology, prognosis, and treatment. *Hematol Oncol Clin North Am.* (2010) 24:65–86. doi: 10.1016/j.hoc.2009.11.011

61. Park JR, Eggert A, Caron H. Neuroblastoma: biology, prognosis, and treatment. *Pediatr Clin N Am.* (2008) 55:97–120. doi: 10.1016/j.pcl.2007.10.014

62. Sharp SE, Trout AT, Weiss BD, Gelfand MJ. MIBG in neuroblastoma diagnostic imaging and therapy. *Radiogr Rev Publ Radiol Soc N Am Inc.* (2016) 36:258–78. doi: 10.1148/rg.2016150099

63. Lumbroso J, Guermazi F, Hartmann O, Coornaert S, Rabarison Y. Sensitivity and specificity of meta-iodobenzylguanidine (mIBG) scintigraphy in the evaluation of neuroblastoma: analysis of 115 cases. *Bull Cancer.* (1988) 75:97–106.

64. Park JR, Bagatell R, Cohn SL, Pearson AD, Villablanca JG, Berthold F. Revisions to the international neuroblastoma response criteria: a consensus statement from the National Cancer Institute clinical trials planning meeting. *J Clin Oncol Off J Am Soc Clin Oncol.* (2017) 35:2580–7. doi: 10.1200/JCO.2016.72.0177

65. Piccardo A, Treglia G, Fiz F, Bar-Sever Z, Bottoni G, Biassoni L. The evidence-based role of catecholaminergic PET tracers in neuroblastoma. A systematic review and a head-to-head comparison with mIBG scintigraphy. *Eur J Nucl Med Mol Imaging.* (2023) 2023:e9. doi: 10.1007/s00259-023-06486-9

66. Decarolis B, Schneider C, Hero B, Simon T, Volland R. Iodine-123 metaiodobenzylguanidine scintigraphy scoring allows prediction of outcome in patients with stage 4 neuroblastoma: results of the Cologne interscore comparison study. *J Clin Oncol Off J Am Soc Clin Oncol.* (2013) 31:944–51. doi: 10.1200/JCO.2012.45.8794

67. Matthay KK, Shulkin B, Ladenstein R, Michon J, Giammarile F. Criteria for evaluation of disease extent by (123)I-metaiodobenzylguanidine scans in neuroblastoma: a report for the international neuroblastoma risk group (INRG) task force. *Br J Cancer.* (2010) 102:1319–26. doi: 10.1038/sj.bjc.6605621

68. Segall G, Delbeke D, Stabin MG, Even-Sapir E, Fair J. SNM practice guideline for sodium 18F-fluoride PET/CT bone scans 1.0. *J Nucl Med Off Publ Soc Nucl Med.* (2010) 51:1813–20. doi: 10.2967/jnumed.110.082263

69. Liu Y, Sheng J, Dong Z, Xu Y, Huang Q, Pan D. The diagnostic performance of 18F-fluoride PET/CT in bone metastases detection: a meta-analysis. *Clin Radiol.* (2019) 74:196–206. doi: 10.1016/j.crad.2018.12.011

70. Sheikhbahaei S, Jones KM, Werner RA, Salas-Fragomeni RA, Marcus CV. 18F-NaF-PET/CT for the detection of bone metastasis in prostate cancer: a meta-analysis of diagnostic accuracy studies. *Ann Nucl Med.* (2019) 33:351–61. doi: 10.1007/s12149-019-01343-y

71. Bénard F, Harsini S, Wilson D, Zukotynski K, Abikhzer G, Turcotte E. Intra-individual comparison of 18F-sodium fluoride PET-CT and 99mTc bone scintigraphy with SPECT in patients with prostate cancer or breast cancer at high risk for skeletal metastases (MITNEC-A1): a multicentre, phase 3 trial. *Lancet Oncol.* (2022) 23:1499–507. doi: 10.1016/S1470-2045(22)00642-8

72. Hillner BE, Siegel BA, Hanna L, Duan F, Shields AF, Coleman RE. Impact of 18F-fluoride PET in patients with known prostate cancer: initial results from the National Oncologic PET registry. *J Nucl Med Off Publ Soc Nucl Med.* (2014) 55:574–81. doi: 10.2967/jnumed.113.130005

73. Zacho HD, Jochumsen MR, Langkilde NC, Mortensen JC, Haarmark C. No added value of 18F-sodium fluoride PET/CT for the detection of bone metastases in patients with newly diagnosed prostate Cancer with Normal bone scintigraphy. *J Nucl Med Off Publ Soc Nucl Med.* (2019) 60:1713–6. doi: 10.2967/jnumed.119.229062

74. Jadvar H, Desai B, Ji L, Conti PS, Dorff TB, Groshen SG. Prospective evaluation of 18F-NaF and 18F-FDG PET/CT in detection of occult metastatic disease in biochemical recurrence of prostate cancer. *Clin Nucl Med.* (2012) 37:637–43. doi: 10.1097/RLU.0b013e318252d829

75. Fonager RF, Zacho HD, Langkilde NC, Fledelius J, Ejlersen JA, Hendel HW. Prospective comparative study of 18F-sodium fluoride PET/CT and planar bone scintigraphy for treatment response assessment of bone metastases in patients with prostate cancer. *Acta Oncol Stockh Swed.* (2018) 57:1063–9. doi: 10.1080/0284186X.2018.1438651

76. Muzi M, O'Sullivan F, Perk TG, Muzi JP, Mankoff DA. Whole-body [18F]-fluoride PET SUV imaging to monitor response to dasatinib therapy in castration-resistant prostate cancer bone metastases: secondary Results from ACRIN 6687. *Tomogr Ann Arbor Mich.* (2021) 7:139–53. doi: 10.3390/tomography7020013

77. Hardcastle N, Hofman MS, Lee CY, Callahan J, Selbie L. NaF PET/CT for response assessment of prostate cancer bone metastases treated with single fraction stereotactic ablative body radiotherapy. *Radiat Oncol Lond Engl.* (2019) 14:164. doi: 10.1186/s13014-019-1359-0

78. Cook G, Parker C, Chua S, Johnson B, Aksnes AK, Lewington VJ. 18F-fluoride PET: changes in uptake as a method to assess response in bone metastases from castrate-resistant prostate cancer patients treated with 223Ra-chloride (Alpharadin). *EJNMMI Res.* (2011) 1:4. doi: 10.1186/2191-219X-1-4

79. Apolo AB, Lindenberg L, Shih JH, Mena E, Kim JW, Park JC. Prospective study evaluating Na18F PET/CT in predicting clinical outcomes and survival in advanced prostate Cancer. *J Nucl Med Off Publ Soc Nucl Med.* (2016) 57:886–92. doi: 10.2967/jnumed.115.166512

80. Azad GK, Siddique M, Taylor B, Green A, O'Doherty J, Gariani J. Is response assessment of breast Cancer bone metastases better with measurement of 18F-fluoride metabolic flux than with measurement of 18F-fluoride PET/CT SUV? *J Nucl Med Off Publ Soc Nucl Med.* (2019) 60:322–7. doi: 10.2967/jnumed.118.208710

81. Azad GK, Taylor BP, Green A, Sandri I, Swampillai A, Harries M. Prediction of therapy response in bone-predominant metastatic breast cancer: comparison of [18F] fluorodeoxyglucose and [18F]-fluoride PET/CT with whole-body MRI with diffusion-weighted imaging. *Eur J Nucl Med Mol Imaging.* (2019) 46:821–30. doi: 10.1007/s00259-018-4223-9

82. Azad GK, Cousin F, Siddique M, Taylor B, Goh V, Cook GJR. Does measurement of first-order and heterogeneity parameters improve response assessment of bone metastases in breast Cancer compared to SUVmax in [18F]fluoride and [18F]FDG PET? *Mol Imaging Biol.* (2019) 21:781–9. doi: 10.1007/s11307-018-1262-3

83. Wade AA, Scott JA, Kuter I, Fischman AJ. Flare response in 18F-fluoride ion PET bone scanning. *AJR Am J Roentgenol.* (2006) 186:1783–6. doi: 10.2214/AJR.05.0225

84. Kairemo K, Joensuu T. Radium-223-dichloride in castration resistant metastatic prostate cancer-preliminary results of the response evaluation using F-18-fluoride PET/CT. *Diagn Basel Switz.* (2015) 5:413–27. doi: 10.3390/diagnostics5040413

85. Kelloff GJ, Hoffman JM, Johnson B, Scher HI, Siegel BA, Cheng EY. Progress and promise of FDG-PET imaging for cancer patient management and oncologic drug development. *Clin Cancer Res Off J Assoc Cancer Res.* (2005) 11:2785–808. doi: 10.1158/1078-0432.CCR-04-2626

86. Castello A, Lopci E. Response assessment of bone metastatic disease: seeing the forest for the trees RECIST, PERCIST, iRECIST, and PCWG-2. *Q J Nucl Med Mol Imaging Off Publ Ital Assoc Nucl Med AIMN Int Assoc Radiopharmacol IAR Sect Soc Of.* (2019) 63:150–8. doi: 10.23736/S1824-4785.19.03193-5

87. Rong J, Wang S, Ding Q, Yun M, Zheng Z, Ye S. Comparison of 18 FDG PET-CT and bone scintigraphy for detection of bone metastases in breast cancer patients. *Surg Oncol.* (2013) 22:86–91. doi: 10.1016/j.suronc.2013.01.002

88. Liu T, Cheng T, Xu W, Yan WL, Liu J, Yang HL. A meta-analysis of 18FDG-PET, MRI and bone scintigraphy for diagnosis of bone metastases in patients with breast cancer. *Skelet Radiol.* (2011) 40:523–31. doi: 10.1007/s00256-010-0963-8

89. van Es SC, Velleman T, Elias SG, Bensch F, Brouwers AH, Glaudemans AWJM. Assessment of bone lesions with 18F-FDG PET compared with 99mTc bone scintigraphy leads to clinically relevant differences in metastatic breast Cancer management. *J Nucl Med Off Publ Soc Nucl Med.* (2021) 62:177–83. doi: 10.2967/jnumed.120.244640

90. de Mooij CM, Ploumen RAW, Nelemans PJ, Mottaghy FM, Smidt ML, van Nijnatten TJA. The influence of receptor expression and clinical subtypes on baseline [18F]FDG uptake in breast cancer: systematic review and meta-analysis. *EJNMMI Res.* (2023) 13:5. doi: 10.1186/s13550-023-00953-y

91. Dashevsky BZ, Goldman DA, Parsons M, Gönen M, Corben AD, Jochelson MS. Appearance of untreated bone metastases from breast cancer on FDG PET/CT: importance of histologic subtype. *Eur J Nucl Med Mol Imaging.* (2015) 42:1666–73. doi: 10.1007/s00259-015-3080-z

92. Bos R, van Der Hoeven JJM, van Der Wall E, van Der Groep P, van Diest PJ. Biologic correlates of (18)fluorodeoxyglucose uptake in human breast cancer measured by positron emission tomography. *J Clin Oncol Off J Am Soc Clin Oncol.* (2002) 20:379–87. doi: 10.1200/JCO.2002.20.2.379

93. Buck A, Schirrmeister H, Kühn T, Shen C, Kalker T, Kotzerke J. FDG uptake in breast cancer: correlation with biological and clinical prognostic parameters. *Eur J Nucl Med Mol Imaging.* (2002) 29:1317–23. doi: 10.1007/s00259-002-0880-8

94. Abe K, Sasaki M, Kuwabara Y, Koga H, Baba S, Hayashi K. Comparison of 18FDG-PET with 99mTc-HMDP scintigraphy for the detection of bone metastases in patients with breast cancer. *Ann Nucl Med.* (2005) 19:573–9. doi: 10.1007/BF02985050

95. Nakai T, Okuyama C, Kubota T, Yamada K, Ushijima Y, Taniike K. Pitfalls of FDG-PET for the diagnosis of osteoblastic bone metastases in patients with breast cancer. *Eur J Nucl Med Mol Imaging.* (2005) 32:1253–8. doi: 10.1007/s00259-005-1842-8

96. Liu Y. The place of FDG PET/CT in renal cell carcinoma: value and limitations. *Front Oncol.* (2016) 6:201. doi: 10.3389/fonc.2016.00201

97. Seo HJ, Kim GM, Kim JH, Kang WJ, Choi HJ. ^{18}F-FDG PET/CT in hepatocellular carcinoma: detection of bone metastasis and prediction of prognosis. *Nucl Med Commun.* (2015) 36:226–33. doi: 10.1097/MNM.0000000000000246

98. Yi X, Fan M, Liu Y, Zhang H, Liu S. 18 FDG PET and PET-CT for the detection of bone metastases in patients with head and neck cancer. A meta-analysis. *J Med Imaging Radiat Oncol.* (2013) 57:674–9. doi: 10.1111/1754-9485.12077

99. Byun BH, Kong CB, Lim I, Kim BI, Choi CW, Song WS. Comparison of (18) F-FDG PET/CT and (99 m)Tc-MDP bone scintigraphy for detection of bone metastasis in osteosarcoma. *Skelet Radiol.* (2013) 42:1673–81. doi: 10.1007/s00256-013-1714-4

100. Stafford SE, Gralow JR, Schubert EK, Rinn KJ, Dunnwald LK. Use of serial FDG PET to measure the response of bone-dominant breast cancer to therapy. *Acad Radiol.* (2002) 9:913–21. doi: 10.1016/S1076-6332(03)80461-0

101. Tateishi U, Gamez C, Dawood S, Yeung HWD, Cristofanilli M, Macapinlac HA. Bone metastases in patients with metastatic breast cancer: morphologic and metabolic monitoring of response to systemic therapy with integrated PET/CT. *Radiology.* (2008) 247:189–96. doi: 10.1148/radiol.2471070567

102. Peterson LM, O'Sullivan J, Wu QV, Novakova-Jiresova A, Jenkins I. Prospective study of serial 18F-FDG PET and 18F-fluoride PET to predict time to skeletal-related events, time to progression, and survival in patients with bone-dominant metastatic breast Cancer. *J Nucl Med Off Publ Soc Nucl Med.* (2018) 59:1823–30. doi: 10.2967/jnumed.118.211102

103. Makhlin I, Korhonen KE, Martin ML, Gillman J, Schubert E, Pantel AR. 18F-FDG PET/CT for the evaluation of therapy response in hormone receptor-positive bone-dominant metastatic breast Cancer. *Radiol Imaging Cancer.* (2022) 4:e220032. doi: 10.1148/rycan.220032

104. Du Y, Cullum I, Illidge TM, Ell PJ. Fusion of metabolic function and morphology: sequential [18F]fluorodeoxyglucose positron-emission tomography/computed tomography studies yield new insights into the natural history of bone metastases in breast cancer. *J Clin Oncol Off J Am Soc Clin Oncol.* (2007) 25:3440–7. doi: 10.1200/JCO.2007.11.2854

105. Vogsen M, Harbo F, Jakobsen NM, Nissen HJ, Dahlsgaard-Wallenius SE, Gerke O. Response monitoring in metastatic breast Cancer: a prospective study comparing 18F-FDG PET/CT with conventional CT. *J Nucl Med Off Publ Soc Nucl Med.* (2023) 64:355–61. doi: 10.2967/jnumed.121.263358

106. Mortimer JE, Dehdashti F, Siegel BA, Trinkaus K, Katzenellenbogen JA, Welch MJ. Metabolic flare: indicator of hormone responsiveness in advanced breast cancer. *J Clin Oncol Off J Am Soc Clin Oncol.* (2001) 19:2797–803. doi: 10.1200/JCO.2001.19.11.2797

107. Krupitskaya Y, Eslamy HK, Nguyen DD, Kumar A, Wakelee HA. Osteoblastic bone flare on F18-FDG PET in non-small cell lung cancer (NSCLC) patients receiving bevacizumab in addition to standard chemotherapy. *J Thorac Oncol Off Publ Int Assoc Study Lung Cancer.* (2009) 4:429–31. doi: 10.1097/JTO.0b013e3181989e12

108. Annunziata S, Pizzuto DA, Treglia G. Diagnostic performance of PET imaging using different radiopharmaceuticals in prostate Cancer according to published Meta-analyses. *Cancers.* (2020) 12:2153. doi: 10.3390/cancers12082153

109. Treglia G, Pereira Mestre R, Ferrari M, Bosetti DG, Pascale M, Oikonomou E. Radiolabelled choline versus PSMA PET/CT in prostate cancer restaging: a meta-analysis. *Am J Nucl Med Mol Imaging.* (2019) 9:127–39.

110. Langsteger W, Balogova S, Huchet V, Beheshti M, Paycha F. Fluorocholine (18F) and sodium fluoride (18F) PET/CT in the detection of prostate cancer: prospective

comparison of diagnostic performance determined by masked reading. *Q J Nucl Med Mol Imaging Off Publ Ital Assoc Nucl Med AIMN Int Assoc Radiopharmacol IAR Sect Soc Of.* (2011) 55:448–57.

111. Wondergem M, van der Zant FM, van der Ploeg T, Knol RJJ. A literature review of 18F-fluoride PET/CT and 18F-choline or 11C-choline PET/CT for detection of bone metastases in patients with prostate cancer. *Nucl Med Commun.* (2013) 34:935–45. doi: 10.1097/MNM.0b013e328364918a

112. Janssen JC, Woythal N, Meißner S, Prasad V, Brenner W. [68Ga]PSMA-HBED-CC uptake in osteolytic, osteoblastic, and bone marrow metastases of prostate Cancer patients. *Mol Imaging Biol.* (2017) 19:933–43. doi: 10.1007/s11307-017-1101-y

113. Pyka T, Okamoto S, Dahlbender M, Tauber R, Retz M, Heck M. Comparison of bone scintigraphy and 68Ga-PSMA PET for skeletal staging in prostate cancer. *Eur J Nucl Med Mol Imaging.* (2016) 43:2114–21. doi: 10.1007/s00259-016-3435-0

114. Hofman MS, Lawrentschuk N, Francis RJ, Tang C, Vela I, Thomas P. Prostate-specific membrane antigen PET-CT in patients with high-risk prostate cancer before curative-intent surgery or radiotherapy (proPSMA): a prospective, randomised, multicentre study. *Lancet Lond Engl.* (2020) 395:1208–16. doi: 10.1016/S0140-6736(20)30314-7

115. Urso L, Filippi L, Castello A, Marzola MC, Bartolomei M, Cittanti C. PSMA PET/CT in castration-resistant prostate Cancer: myth or reality? *J Clin Med.* (2023) 12:7130. doi: 10.3390/jcm12227130

116. Fanti S, Minozzi S, Castellucci P, Balduzzi S, Herrmann K, Krause BJ. PET/CT with (11)C-choline for evaluation of prostate cancer patients with biochemical recurrence: meta-analysis and critical review of available data. *Eur J Nucl Med Mol Imaging.* (2016) 43:55–69. doi: 10.1007/s00259-015-3202-7

117. Guo Y, Wang L, Hu J, Feng D, Xu L. Diagnostic performance of choline PET/CT for the detection of bone metastasis in prostate cancer: a systematic review and meta-analysis. *PLoS One.* (2018) 13:e0203400. doi: 10.1371/journal.pone.0203400

118. Afshar-Oromieh A, Zechmann CM, Malcher A, Eder M, Eisenhut M, Linhart HG. Comparison of PET imaging with a (68)Ga-labelled PSMA ligand and (18) F-choline-based PET/CT for the diagnosis of recurrent prostate cancer. *Eur J Nucl Med Mol Imaging.* (2014) 41:11–20. doi: 10.1007/s00259-013-2525-5

119. Schwenck J, Rempp H, Reischl G, Kruck S, Stenzl A. Comparison of 68Ga-labelled PSMA-11 and 11C-choline in the detection of prostate cancer metastases by PET/CT. *Eur J Nucl Med Mol Imaging.* (2017) 44:92–101. doi: 10.1007/s00259-016-3490-6

120. Burgard C, Hoffmann MA, Frei M, Buchholz HG, Khreish F, Marlowe RJ. Detection efficacy of 68Ga-PSMA-11 PET/CT in biochemical recurrence of prostate Cancer with very Low PSA levels: a 7-year, two-center "real-world" experience. *Cancers.* (2023) 15:1376. doi: 10.3390/cancers15051376

121. Perera M, Papa N, Roberts M, Williams M, Udovicich C, Vela I. Gallium-68 prostate-specific membrane antigen positron emission tomography in advanced prostate Cancer-updated diagnostic utility, sensitivity, specificity, and distribution of prostate-specific membrane antigen-avid lesions: a systematic review and Meta-analysis. *Eur Urol.* (2020) 77:403–17. doi: 10.1016/j.eururo.2019.01.049

122. Castellucci P, Ceci F, Graziani T, Schiavina R, Brunocilla E. Early biochemical relapse after radical prostatectomy: which prostate cancer patients may benefit from a restaging 11C-choline PET/CT scan before salvage radiation therapy? *J Nucl Med Off Publ Soc Nucl Med.* (2014) 55:1424–9. doi: 10.2967/jnumed.114.138313

123. Afshar-Oromieh A, Holland-Letz T, Giesel FL, Kratochwil C, Mier W, Haufe S. Diagnostic performance of 68Ga-PSMA-11 (HBED-CC) PET/CT in patients with recurrent prostate cancer: evaluation in 1007 patients. *Eur J Nucl Med Mol Imaging.* (2017) 44:1258–68. doi: 10.1007/s00259-017-3711-7

124. Schwarzenböck SM, Knieling A, Souvatzoglou M, Kurth J, Steiger K, Eiber M. [11C]choline PET/CT in therapy response assessment of a neoadjuvant therapy in locally advanced and high risk prostate cancer before radical prostatectomy. *Oncotarget.* (2016) 7:63747–57. doi: 10.18632/oncotarget.11653

125. Fanti S, Hadaschik B, Herrmann K. Proposal for systemic-therapy response-assessment criteria at the time of PSMA PET/CT imaging: the PSMA PET progression criteria. *J Nucl Med Off Publ Soc Nucl Med.* (2020) 61:678–82. doi: 10.2967/jnumed.119.233817

126. Gafita A, Rauscher I, Weber M, Hadaschik B, Wang H. Novel framework for treatment response evaluation using PSMA PET/CT in patients with metastatic castration-resistant prostate Cancer (RECIP 1.0): an international multicenter study. *J Nucl Med Off Publ Soc Nucl Med.* (2022) 63:1651–8. doi: 10.2967/jnumed.121.263072

127. Gafita A, Rauscher I, Fendler WP, Murthy V, Hui W, Armstrong WR. Measuring response in metastatic castration-resistant prostate cancer using PSMA PET/CT: comparison of RECIST 1.1, aPCWG3, aPERCIST, PPP, and RECIP 1.0 criteria. *Eur J Nucl Med Mol Imaging.* (2022) 49:4271–81. doi: 10.1007/s00259-022-05882-x

128. Probst C, Bjartell A, Anand A, Skamene T, Ferrario C. Interval changes in PSMA PET/CT during Radium-223 therapy for metastatic bone disease from castration-resistant prostate Cancer. *Nucl Med Mol Imaging.* (2022) 56:188–95. doi: 10.1007/s13139-022-00754-6

129. Castello A, Macapinlac HA, Lopci E, Santos EB. Prostate-specific antigen flare induced by 223RaCl2 in patients with metastatic castration-resistant prostate cancer. *Eur J Nucl Med Mol Imaging.* (2018) 45:2256–63. doi: 10.1007/s00259-018-4051-y

130. Schmidkonz C, Cordes M, Goetz TI, Prante O, Kuwert T, Ritt P. 68Ga-PSMA-11 PET/CT derived quantitative volumetric tumor parameters for classification and

131. Conteduca V, Poti G, Caroli P, Russi S, Brighi N, Lolli C. Flare phenomenon in prostate cancer: recent evidence on new drugs and next generation imaging. *Ther Adv Med Oncol.* (2021) 13:175883592098765. doi: 10.1177/1758835920987654

132. Aggarwal R, Wei X, Kim W, Small EJ, Ryan CJ, Carroll P. Heterogeneous flare in prostate-specific membrane antigen positron emission tomography tracer uptake with initiation of androgen pathway blockade in metastatic prostate Cancer. *Eur Urol Oncol.* (2018) 1:78–82. doi: 10.1016/j.euo.2018.03.010

133. Zacho HD, Petersen LJ. Bone flare to androgen deprivation therapy in metastatic, hormone-sensitive prostate Cancer on 68Ga-prostate-specific membrane antigen PET/CT. *Clin Nucl Med.* (2018) 43:e404–6. doi: 10.1097/RLU.0000000000002273

134. Plouznikoff N, Artigas C, Sideris S, Martinez Chanza N, Gil T. Evaluation of PSMA expression changes on PET/CT before and after initiation of novel antiandrogen drugs (enzalutamide or abiraterone) in metastatic castration-resistant prostate cancer patients. *Ann Nucl Med.* (2019) 33:945–54. doi: 10.1007/s12149-019-01404-2

135. Cives M, Strosberg JR. Gastroenteropancreatic neuroendocrine tumors. *CA Cancer J Clin.* (2018) 68:471–87. doi: 10.3322/caac.21493

136. Dasari A, Shen C, Halperin D, Zhao B, Zhou S, Xu Y. Trends in the incidence, prevalence, and survival outcomes in patients with neuroendocrine tumors in the United States. *JAMA Oncol.* (2017) 3:1335–42. doi: 10.1001/jamaoncol.2017.0589

137. Kavecansky J, Wei L, Caronia L, Ramirez MT, Bloomston M, Shah MH. Bone metastases in well-to-moderately differentiated neuroendocrine tumors: a single institutional review from the Ohio State University medical center. *Pancreas.* (2015) 44:198–203. doi: 10.1097/MPA.0000000000000267

138. Van Loon K, Zhang L, Keiser J, Carrasco C, Glass K. Bone metastases and skeletal-related events from neuroendocrine tumors. *Endocr Connect.* (2015) 4:9–17. doi: 10.1530/EC-14-0119

139. Scharf M, Petry V, Daniel H, Rinke A, Gress TM. Bone metastases in patients with neuroendocrine neoplasm: frequency and clinical, therapeutic, and prognostic relevance. *Neuroendocrinology.* (2018) 106:30–7. doi: 10.1159/000457954

140. Riihimäki M, Hemminki A, Sundquist K, Sundquist J, Hemminki K. The epidemiology of metastases in neuroendocrine tumors. *Int J Cancer.* (2016) 139:2679–86. doi: 10.1002/ijc.30400

141. Peri M, Botteri E, Pisa E, De Marinis F, Ungaro A. A single-institution retrospective analysis of metachronous and synchronous metastatic bronchial neuroendocrine tumors. *J Thorac Dis.* (2018) 10:3928–39. doi: 10.21037/jtd.2018.06.78

142. Gibril F, Doppman JL, Reynolds JC, Chen CC, Sutliff VE, Yu F. Bone metastases in patients with gastrinomas: a prospective study of bone scanning, somatostatin receptor scanning, and magnetic resonance image in their detection, frequency, location, and effect of their detection on management. *J Clin Oncol Off J Am Soc Clin Oncol.* (1998) 16:1040–53. doi: 10.1200/JCO.1998.16.3.1040

143. Scarsbrook AF, Ganeshan A, Statham J, Thakker RV, Weaver A, Talbot D. Anatomic and functional imaging of metastatic carcinoid tumors. *Radiogr Rev Publ Radiol Soc N Am Inc.* (2007) 27:455–77. doi: 10.1148/rg.272065058

144. Meijer WG, van der Veer E, Jager PL, van der Jagt EJ, Piers BA. Bone metastases in carcinoid tumors: clinical features, imaging characteristics, and markers of bone metabolism. *J Nucl Med Off Publ Soc Nucl Med.* (2003) 44:184–91.

145. Panzuto F, Pusceddu S, Faggiano A, Rinzivillo M, Brighi N, Prinzi N. Prognostic impact of tumour burden in stage IV neuroendocrine neoplasia: a comparison between pancreatic and gastrointestinal localizations. *Pancreatol Off J Int Assoc Pancreatol IAP Al.* (2019) 19:1067–73. doi: 10.1016/j.pan.2019.09.015

146. Cives M, Rizzo F, Simone V, Bisceglia F, Stucci S, Seeber A. Reviewing the Osteotropism in neuroendocrine tumors: the role of epithelial-mesenchymal transition. *Neuroendocrinology.* (2016) 103:321–34. doi: 10.1159/000438902

147. Alexandraki KI, Pizanias M, Uri I, Thomas D, Page T, Kolomodi D. The prognosis and management of neuroendocrine neoplasms-related metastatic bone disease: lessons from clinical practice. *Endocrine.* (2019) 64:690–701. doi: 10.1007/s12020-019-01838-8

148. Cives M, Pellè E, Rinzivillo M, Prosperi D, Tucci M, Silvestris F. Bone metastases in neuroendocrine tumors: molecular pathogenesis and implications in clinical practice. *Neuroendocrinology.* (2021) 111:207–16. doi: 10.1159/000508633

149. Deroose CM, Hindié E, Kebebew E, Goichot B, Pacak K. Molecular imaging of Gastroenteropancreatic neuroendocrine tumors: current status and future directions. *J Nucl Med Off Publ Soc Nucl Med.* (2016) 57:1949–56. doi: 10.2967/jnumed.116.179234

150. Rust E, Hubele F, Marzano E, Goichot B, Pessaux P, Kurtz JE. Nuclear medicine imaging of gastro-entero-pancreatic neuroendocrine tumors. The key role of cellular differentiation and tumor grade: from theory to clinical practice. *Cancer Imaging Off Publ Int Cancer Imaging Soc.* (2012) 12:173–84. doi: 10.1102/1470-7330.2012.0026

151. Merola E, Pavel ME, Panzuto F, Capurso G, Cicchese N, Rinke A. Functional imaging in the follow-up of Enteropancreatic neuroendocrine tumors: clinical usefulness and indications. *J Clin Endocrinol Metab.* (2017) 102:1486–94. doi: 10.1210/jc.2016-3732

152. Albanus DR, Apitzsch J, Erdem Z, Erdem O, Verburg FA, Behrendt FF. Clinical value of ⁶⁸Ga-DOTATATE-PET/CT compared to stand-alone contrast enhanced CT for the detection of extra-hepatic metastases in patients with neuroendocrine tumours (NET). *Eur J Radiol.* (2015) 84:1866–72. doi: 10.1016/j.ejrad.2015.06.024

153. Gauthé M, Testart Dardel N, Ruiz Santiago F, Ohnona J, Nataf V, Montravers F. Vertebral metastases from neuroendocrine tumours: how to avoid false positives on 68Ga-DOTA-TOC PET using CT pattern analysis? *Eur Radiol.* (2018) 28:3943–52. doi: 10.1007/s00330-017-5294-x

154. Ambrosini V, Nanni C, Zompatori M, Campana D, Tomassetti P. (68)Ga-DOTA-NOC PET/CT in comparison with CT for the detection of bone metastasis in patients with neuroendocrine tumours. *Eur J Nucl Med Mol Imaging.* (2010) 37:722–7. doi: 10.1007/s00259-009-1349-9

155. Skoura E, Michopoulou S, Mohmaduvesh M, Panagiotidis E, Al Harbi M. The impact of 68Ga-DOTATATE PET/CT imaging on Management of Patients with neuroendocrine tumors: experience from a National Referral Center in the United Kingdom. *J Nucl Med Off Publ Soc Nucl Med.* (2016) 57:34–40. doi: 10.2967/jnumed.115.166017

156. Crown A, Rocha FG, Raghu P, Lin B, Funk G, Alseidi A. Impact of initial imaging with gallium-68 dotatate PET/CT on diagnosis and management of patients with neuroendocrine tumors. *J Surg Oncol.* (2020) 121:480–5. doi: 10.1002/jso.25812

157. Strosberg J, El-Haddad G, Wolin E, Hendifar A, Yao J. Phase 3 trial of 177Lu-Dotatate for midgut neuroendocrine tumors. *N Engl J Med.* (2017) 376:125–35. doi: 10.1056/NEJMoa1607427

158. Kennedy J, Chicheportiche A, Keidar Z. Quantitative SPECT/CT for dosimetry of peptide receptor radionuclide therapy. *Semin Nucl Med.* (2022) 52:229–42. doi: 10.1053/j.semnuclmed.2021.11.004

159. Ezziddin S, Sabet A, Heinemann F, Yong-Hing CJ, Ahmadzadehfar H, Guhlke S. Response and long-term control of bone metastases after peptide receptor radionuclide therapy with (177)Lu-octreotate. *J Nucl Med Off Publ Soc Nucl Med.* (2011) 52:1197–203. doi: 10.2967/jnumed.111.090373

160. Sabet A, Khalaf F, Haslerud T, Al-Zreiqat A, Sabet A. Bone metastases in GEP-NET: response and long-term outcome after PRRT from a follow-up analysis. *Am J Nucl Med Mol Imaging.* (2013) 3:437–45.

161. Imperiale A, Meuter L, Pacak K, Taïeb D. Variants and pitfalls of PET/CT in neuroendocrine tumors. *Semin Nucl Med.* (2021) 51:519–28. doi: 10.1053/j.semnuclmed.2021.03.001

162. Minn H, Kauhanen S, Seppänen M, Nuutila P. 18F-FDOPA: a multiple-target molecule. *J Nucl Med Off Publ Soc Nucl Med.* (2009) 50:1915–8. doi: 10.2967/jnumed.109.065664

163. Taïeb D, Imperiale A, Pacak K. (18)F-DOPA: the versatile radiopharmaceutical. *Eur J Nucl Med Mol Imaging.* (2016) 43:1187–9. doi: 10.1007/s00259-016-3354-0

164. Koopmans KP, de Vries EGE, Kema IP, Elsinga PH, Neels OC, Sluiter WJ. Staging of carcinoid tumours with 18F-DOPA PET: a prospective, diagnostic accuracy study. *Lancet Oncol.* (2006) 7:728–34. doi: 10.1016/S1470-2045(06)70801-4

165. Becherer A, Szabó M, Karanikas G, Wunderbaldinger P, Angelberger P. Imaging of advanced neuroendocrine tumors with (18)F-FDOPA PET. *J Nucl Med Off Publ Soc Nucl Med.* (2004) 45:1161–7.

166. Deleval N, Pesque L, Dieudonné A, Viry F, Hentic O, Lebtahi R. Prognostic impact of bone metastases detected by 18F-DOPA PET in patients with metastatic midgut neuroendocrine tumors. *Eur Radiol.* (2021) 31:4166–74. doi: 10.1007/s00330-020-07554-6

167. Lelièvre M, Triumbari EKA, Brixi H, Perrier M, Cadiot G, Deguelte S. Bone metastases in midgut neuroendocrine tumors: imaging characteristics, distribution, and risk factors. *Endocrine.* (2022) 78:380–6. doi: 10.1007/s12020-022-03160-2

168. Ouvrard E, Chevalier E, Addeo P, Sahakian N, Detour J, Goichot B. Intraindividual comparison of 18 F-FDOPA and 68 Ga-DOTATOC PET/CT detection rate for metastatic assessment in patients with ileal neuroendocrine tumours. *Clin Endocrinol.* (2021) 94:66–73. doi: 10.1111/cen.14312

169. Veenstra EB, de Groot DJA, Brouwers AH, Walenkamp AME, Noordzij W. Comparison of 18F-DOPA versus 68Ga-DOTATOC as preferred PET imaging tracer in well-differentiated neuroendocrine neoplasms. *Clin Nucl Med.* (2021) 46:195–200. doi: 10.1097/RLU.0000000000003447

170. Ansquer C, Touchefeu Y, Faivre-Chauvet A, Leux C, Le Bras M. Head-to-head comparison of 18F-DOPA PET/CT and 68Ga-DOTANOC PET/CT in patients with midgut neuroendocrine tumors. *Clin Nucl Med.* (2021) 46:181–6. doi: 10.1097/RLU.0000000000003450

171. Ouvrard E, Mestier LD, Boursier C, Lachachi B, Sahakian N, Chevalier E. 18F-DOPA PET/CT at the forefront of initial or Presurgical evaluation of Small-intestine neuroendocrine tumors. *J Nucl Med Off Publ Soc Nucl Med.* (2022) 63:1865–70. doi: 10.2967/jnumed.122.263984

172. Piccardo A, Fiz F, Bottoni G, Ugolini M, Noordzij W, Trimboli P. Head-to-head comparison between 18 F-DOPA PET/CT and 68 Ga-DOTA peptides PET/CT in detecting intestinal neuroendocrine tumours: a systematic review and meta-analysis. *Clin Endocrinol.* (2021) 95:595–605. doi: 10.1111/cen.14527

173. Binderup T, Knigge U, Johnbeck CB, Loft A, Berthelsen AK, Oturai P. 18F-FDG PET is superior to WHO grading as a prognostic tool in neuroendocrine neoplasms and useful in guiding PRRT: a prospective 10-year follow-up study. *J Nucl Med Off Publ Soc Nucl Med.* (2021) 62:808–15. doi: 10.2967/jnumed.120.244798